May 2022
Report No. 22-031



# Automated Guardrail Inventory and Condition Evaluation

Principal Investigator (s)
Dr. Chengbo Ai

University of Massachusetts Amherst

Research and Technology Transfer Section
MassDOT Office of Transportation Planning

U.S. Department of Transportation
Federal Highway Administration

# Technical Report Document Page

| 1. Report No. | 2. Government Accession No. | 3. Recipient's Catalog No. |
|---|---|---|
| 22-031 | | |

| 4. Title and Subtitle | 5. Report Date |
|---|---|
| Automated Guardrail Inventory and Condition Evaluation | May 2022 |
| | 6. Performing Organization Code |

| 7. Author(s) | 8. Performing Organization Report No. |
|---|---|
| Chengbo Ai and Qing Hou | 22-031 |

| 9. Performing Organization Name and Address | 10. Work Unit No. (TRAIS) |
|---|---|
| University of Massachusetts Amherst 130 Natural Resources Way, Amherst, MA 01003 | 11. Contract or Grant No. |

| 12. Sponsoring Agency Name and Address | 13. Type of Report and Period Covered |
|---|---|
| Massachusetts Department of Transportation<br>Office of Transportation Planning<br>Ten Park Plaza, Suite 4150, Boston, MA 02116 | Final Report – May 2022<br>[January 2021 - May 2022] |
| | 14. Sponsoring Agency Code<br>n/a |

15. Supplementary Notes

Project Champion – Neil Boudreau, MassDOT

16. Abstract

MassDOT actively works with FHWA on the Manual for Assessing Safety Hardware (MASH) implementation. It is critical to plan and manage MASH upgrades and integrate the guardrail asset within its asset management plan with a complete guardrail inventory. This study aims at developing and validating new processes using automated methods to identify and extract locations of in-service guardrails and evaluate condition and compliance using pilot-testing road sections. The detailed objectives include: 1) Developing an automated method for determining the presence of guardrails along the roadway and for extracting critical information, including georeferenced starting and ending points, terminal types, curb presence, lateral offset, and elevation; and 2) Developing an automated method for identifying typical conditional changes for guardrails, including face dent, end terminal damage/missing, guardrail support deficiency. The research team has also investigated the feasibility of identifying missing bolts and connection failures using image processing. The deliverables include a georeferenced guardrail inventory for the selected pilot-testing sections, integrating the in-service condition information.

| 17. Key Word | 18. Distribution Statement |
|---|---|
| MASH upgrades, guardrails, LiDAR, condition, compliance | |

| 19. Security Classif. (of this report) | 20. Security Classif. (of this page) | 21. No. of Pages | 22. Price |
|---|---|---|---|
| unclassified | unclassified | 67 | n/a |

**Form DOT F 1700.7** (8-72) Reproduction of completed page authorized

# Automated Guardrail Inventory and Condition Evaluation

Final Report

Prepared By:

**Dr. Chengbo Ai**
Principal Investigator

**Qing Hou**
Researcher

Civil and Environmental Engineering
University of Massachusetts Amherst
130 Natural Resources Rd., Amherst, MA 01003

Prepared For:

Massachusetts Department of Transportation
Office of Transportation Planning
Ten Park Plaza, Suite 4150
Boston, MA 02116

May 2022

# Acknowledgments

Prepared in cooperation with the Massachusetts Department of Transportation, Office of Transportation Planning, and the United States Department of Transportation, Federal Highway Administration.

The Project Team would like to acknowledge the efforts of Mr. Neil Boudreau, Mr. Corey O'Connor, Mr. Jack Moran, and Mr. Evin O'Sullivan from the Highway Division at MassDOT, Ms. Lily Oliver from the Office of Transportation Planning at MassDOT, and Dr. Michael Knodler, Mr. Matt Mann, Ms. Kimberley Foster from the UMass Transportation Center, for their continuous financial, technical, and administrative supports. The Project Team would also like to acknowledge the effort of research members Mr. Kabir Khurana and Ms. Emily Hennessy from UMass Amherst.

# Disclaimer

This page left blank intentionally.

# Executive Summary

This study of "Automated Guardrail Inventory and Condition Evaluation" was undertaken as part of the Massachusetts Department of Transportation (MassDOT) Research Program. This program is funded with Federal Highway Administration (FHWA) State Planning and Research (SPR) funds. Through this program, applied research is conducted on topics of importance to the Commonwealth of Massachusetts transportation agencies.

This study is aimed at developing and validating new processes using automated light detection and ranging (LiDAR) and video-log imagery to identify and extract locations of in-service guardrails and evaluate condition and compliance using representative pilot-testing road sections. Representative testing sections of interstate and non-interstate roadways, with various lengths and guardrail coverages, were selected and analyzed within the study. The detailed objectives include:

- Develop an automated method for determining the presence of guardrails along the roadway and for extracting critical information, including georeferenced starting and ending points, terminal types, curb presence, lateral offset (from the edge of the nearest travel lane to the guardrail), and elevation (from the pavement surface to the tip of the guardrail).
- Develop an automated method for identifying typical conditional changes for guardrails, including face dentation, end terminal damage/missing, and guardrail support deficiency. The research team investigated the feasibility of identifying missing bolts or connection failure of guardrails using image processing.

The deliverables of this study include a georeferenced (and linearly referenced) guardrail inventory for the selected pilot-testing sections, integrating the in-service presence and condition information to support evaluation for MASH compliance and network-level maintenance strategy.

The outcome of this study is summarized as follows:

- *A Review of Guardrail Inventory Efforts*. The research team conducted a detailed literature review of available and ongoing research through Transport Research International Documentation (TRID) on guardrail inventory and condition evaluation methods and mobile LiDAR applications, as well as the existing effort of guardrail data collection and inventory that is made by MassDOT.
- *Mobile LiDAR Data Acquisition*. The research team conducted a comprehensive data acquisition and data preprocessing using the mobile LiDAR sensor (i.e., Riegl VMZ-2000) along with the selected, representative, pilot-testing routes.

    - The collected data cover more than 62 miles of different classifications of highways. An additional 15 miles of the network near Worcester, MA, covering State Route 9, State Route 12, and State Route 122, were scanned to demonstrate the overall performance and feasibility of the developed methodology.

- *Guardrail Inventory*. The research team developed fully automated LiDAR processing algorithms for identifying the locations (starting and ending) along the selected pilot-testing routes.
    - The overall performance for the inventory algorithm shows precisions of 0.956 and 0.955 and recalls of 0.957 and 0.944 along the two testing sections on State Route 9 and State Route 113, respectively.
    - The productivity (i.e., the processing time) was also evaluated to assess the feasibility of applying the proposed method to a statewide process. On average, the processing rate for the guardrail inventory algorithm is at approximately 150 seconds per mile.
- *Guardrail Property Extraction*. The research team developed a suite of automated algorithms to extract the detailed properties of the inventoried guardrails, including terminal types, curb presence, lateral offset (from the edge of the nearest travel lane to the guardrail), and elevations (from the pavement surface and ground with curb to the tip of the guardrail).
    - For terminal type identification, three categories of terminals can be successfully extracted and classified, including buried-in-backslope (BIB) terminal, curved terminal (e.g., Modified Eccentric Loader Terminal (MELT), Regent-C, Slotted Rail Termina (SRT-350), etc.), flat terminal (e.g., Flared Energy-Absorbing Terminal (FLEAT), Sequential Kinking Terminal (SKT), Extruder Terminal (ET-Plus), etc.). Out of the tested 427 terminals, the accuracy of the classification rate is 96.4%, with only nine BIB terminals misclassified as curved terminals.
    - For geometry property extraction, the developed algorithms can accurately measure the lateral offset and elevations of the guardrail with an average error of less than 1/2 inch. Specifically, by identifying the curb presence, the elevations of guardrails can be measured from the tip to both the pavement surface and the curbed ground with consistent accuracy.
    - The productivity (i.e., the processing time) was also evaluated to assess the feasibility of applying the proposed method to a statewide process. On average, the processing rate for the guardrail property extraction algorithm is at approximately 45 seconds per mile.
- *Guardrail Condition Assessment*. The research team developed a suite of automated algorithms to assess the conditions of the inventoried guardrails, including face dentation, terminal damage/missing, and support deficiency. The research team also investigated the

feasibility of identifying missing bolts or connection failure of guardrails using image processing.

  - For face dentation and terminal damage/missing, the algorithms are evaluated on a 5-mile section along State Route 2, and all of the 16 locations with face dentations and 2 locations with deficient supports were successfully located.
  - For terminal damage identification, although no damaged/missing terminals were found in the collected data, the terminal classification algorithm has clearly shown its feasibility of the algorithm. In this study, any terminals that are not identified as BIB, curved or flat terminals will be classified as damaged/missing terminals.
  - For missing/loosened bolt identification, although no missing bolts were found in the collected data, the algorithm using datasets collected from previous studies has shown the feasibility of automatically identifying the locations of bolts from video log images using the developed machine learning algorithm. However, due to the configuration of the camera (i.e., the distance between the sensor and the guardrail, the current resolution of 1920x1080 may not be sufficient to identify missing/loosened bolts, and future studies remain needed to further validate the feasibility.
  - The productivity (i.e., the processing time) was also evaluated to assess the feasibility of applying the proposed method to a statewide process. On average, the processing rate for the guardrail condition assessment algorithm is at approximately 60 seconds per mile.

- *Development and validation of the fully automated guardrail inventory and condition evaluation methodology*. The research team has developed a comprehensive methodology for automatically inventorying the locations of the in-service guardrails, extracting the corresponding properties and conditions, and leveraging mobile LiDAR point cloud data and video log images. A case study covering 15 miles of the network (including State Route 9, State Route 12, and State Route 122) near Worcester, MA, was developed to demonstrate the feasibility of the developed methodology for network-level analysis. The resulting inventory geodatabase with all the properties and conditions can be readily used for supporting asset management and safety improvement tasks for MassDOT.

This page left blank intentionally.

# Table of Contents

This page left blank intentionally.

# List of Figures

This page left blank intentionally.

# List of Acronyms

| Acronym | Expansion |
|---|---|
| AASHTO | American Association of State Highway and Transportation Officials |
| BIB | Buried-In-Backslope |
| CNN | Convolutional Neural Network |
| DBSCAN | Density-Based Spatial Clustering of Applications with Noise |
| DoN | Difference of Normal |
| ECEF | Earth-Center Earth-Fixed |
| FHWA | Federal Highway Administration |
| FLEAT | Flared Energy-Absorbing Terminal |
| GIS | Geographic Information System |
| GPS | Global Positioning System |
| IMU | Inertial Measurement Unit |
| LiDAR | Light Detection and Ranging |
| MASH | Manual for Assessing Safety Hardware |
| MassDOT | Massachusetts Department of Transportation |
| NCHRP | National Cooperative Highway Research Program |
| PCA | Principal Component Analysis |
| RANSAC | RANdom SAmple Consensus |
| ROI | Region Of Interest |
| SKT | Sequential Kinking Terminal |
| SPR | State Planning and Research |
| TRID | Transport Research International Documentation |
| AASHTO | American Association of State Highway and Transportation Officials |

This page left blank intentionally.

# 1.0 Introduction

This study of "Automated Guardrail Inventory and Condition Evaluation" was undertaken as part of the Massachusetts Department of Transportation (MassDOT) Research Program. This program is funded with Federal Highway Administration (FHWA) State Planning and Research (SPR) funds. Through this program, applied research is conducted on topics of importance to the Commonwealth of Massachusetts transportation agencies.

## 1.1 Background

Guardrail is an important boundary infrastructure that provides effective prevention for vehicles running out of the road and protects critical roadside properties from consequential collisions (*1*). The presence and condition of the installed guardrails are vital for roadway safety. Many public transportation agencies, including MassDOT, are responsible for a large inventory of guardrails and are responsible for making timely repairs or replacements of damaged or missing components. The recent issuance of the Manual for Assessing Safety Hardware (MASH) by the American Association of State Highway and Transportation Officials (AASHTO) also presents a need for modernization of the inventory. For contracts on the National Highway System with a letting date after the (final sunset date: December 31, 2019) dates, only safety hardware evaluated using the 2016 edition of MASH criteria will be allowed for new permanent installations and full replacements with limited exceptions (*2*). State DOTs are actively working with FHWA on the implementation of MASH hardware. Therefore, it is critical for state departments of transportation, e.g., MassDOT, to develop a comprehensive guardrail inventory to better plan and manage MASH upgrades and integrate the guardrail asset class within the State transportation asset management plan.

Many transportation agencies have invested numerous resources and efforts in establishing accurate and up-to-date guardrail inventories in their jurisdictions. Although the rich datasets of guardrail information have been acquired through these guardrail inventorying efforts, these methods, predominantly manual approaches, remain labor-intensive, time-consuming, and subjective. Also, many conditional defects may easily be overlooked during the windshield survey. Therefore, improving the efficiency and accuracy of the guardrail inventory process becomes urgent.

With the advancement of mobile light detection and ranging (LiDAR) and computer vision, it has become feasible for state transportation agencies to leverage the widely available data for a cost-effective and efficient method for inventorying and updating guardrail condition information. Although some efforts have been made for automation using image processing

and LiDAR, they only focused on the locations of the guardrails, where the critical properties are still lacking. 2) None of the previous studies focused on the condition of the guardrails. Although a certain level of automation has been achieved using LiDAR and imagery, manual review and digitization remain essential for visual defect identification. Therefore, exploring the feasibility and efficiency of automated guardrail inventory and condition evaluation methods, leveraging the emerging LiDAR and computer vision technologies, becomes necessary.

## 1.2 Objectives and Detailed Tasks

This study is aimed at developing and validating new processes using automated LiDAR and video-log imagery to identify and extract locations of in-service guardrails and evaluate condition and compliance using representative pilot-testing road sections. Representative testing sections of interstate and non-interstate roadways, with various lengths and guardrail coverages, were selected and analyzed within the study. The detailed objectives include:

- Develop an automated method for determining the presence of guardrails along the roadway and for extracting critical information, including georeferenced starting and ending points, terminal types, curb presence, lateral offset (from the edge of the nearest travel lane to the guardrail), and elevation (from the pavement surface to the tip of the guardrail).
- Develop an automated method for identifying typical conditional changes for guardrails, including face dentation, end terminal damage/missing, and guardrail support deficiency. The research team investigated the feasibility of identifying missing bolts or connection failure of guardrails using image processing.

The deliverables of this study include a georeferenced (and linearly referenced) guardrail inventory for the selected pilot-testing sections, integrating the in-service presence and condition information to support evaluation for MASH compliance and network-level maintenance strategy. To achieve the proposed objectives of this study, the detailed work tasks are listed as follows:

- Task 1: Review of Guardrail Inventory Efforts. The research team conducted a detailed literature review of available and ongoing research through Transport Research International Documentation (TRID) on guardrail inventory and condition evaluation methods and mobile LiDAR applications, as well as the existing effort of guardrail data collection and inventory that is made by MassDOT.

- Task 2: Mobile LiDAR Data Acquisition. The research team conducted a comprehensive data acquisition and data preprocessing using the mobile LiDAR sensor (i.e., Riegl VMZ-2000) along with the selected, representative, pilot-testing routes.
- Task 3: Data Processing for Identifying Guardrail Locations. The research team developed computer-aided LiDAR processing algorithms for identifying the locations (starting and ending) along the selected pilot-testing routes. The productivity (i.e., the processing time) was also evaluated to assess the feasibility of applying the proposed method to a statewide process.
- Task 4: Data Processing for Extracting Guardrail Properties. The research team developed computer-aided algorithms to extract the detailed properties of the inventoried guardrails from Task 3, including terminal types, curb presence, lateral offset (from the edge of the nearest travel lane to the guardrail), and elevation (from the pavement surface to the tip of the guardrail). The productivity (i.e., the processing time) was also evaluated to assess the feasibility of applying the proposed method to a statewide process.
- Task 5: Data Processing for Evaluating Guardrail Conditions. The research team developed computer vision algorithms to evaluate the conditions of the inventoried guardrails from Tasks 3 and 4, including face dentation, end terminal damage/missing, and guardrail support deficiency. The research team also investigated the feasibility of identifying missing bolts or connection failure of guardrails using image processing. Besides safety improvement applications, the research team also demonstrated the possible application in asset management using the derived guardrail locations and conditions. The productivity (i.e., the processing time was also evaluated to assess the feasibility of applying the proposed method to a statewide process.
- Task 6: Reporting of Results. The research team prepared the final report and the corresponding PowerPoint-based project presentation with all the technical details.

## 1.3 Organization of this Report

This report is organized as follows. Section 1 introduced the background, research needs, objectives, and detailed work tasks of this research project. Section 2 presents the methodology for processing the mobile LiDAR data for inventory and condition information extraction. Section 3 presents the results of the developed algorithms. Section 4 summarizes the findings and results of this project and recommends the future study.

This page left blank intentionally.

# 2.0 Research Methodology

The research methodology for this study consisted of four main parts: a review of existing technologies, the collection of mobile LiDAR and video log image data, and the processing of the mobile LiDAR and video log image data. Subsection 2.1 presents an overview of the research methodology. Subsection 2.2 presents the details of the mobile LiDAR and video log image data acquisition, followed by Subsections 2.3 through 2.5 that describe the algorithms for automated guardrail extraction, properties extraction, and condition evaluation using mobile LiDAR point clouds and video log images. It should be noted that all the relevant literature reviews are presented in the corresponding subsections.

## 2.1 Methodology Overview

In this study, a complete data processing methodology for guardrail inventory from raw LiDAR and video log image data acquisition to GIS integration. The methodology consists of five key steps, including data acquisition, guardrail location identification, guardrail property extraction, guardrail condition evaluation, and the final guardrail inventory and GIS integration. Figure 2.1 shows an overview of the research methodology. The subsequent sections present the detailed methods and algorithms developed in this study for each key step of this complete data processing methodology.

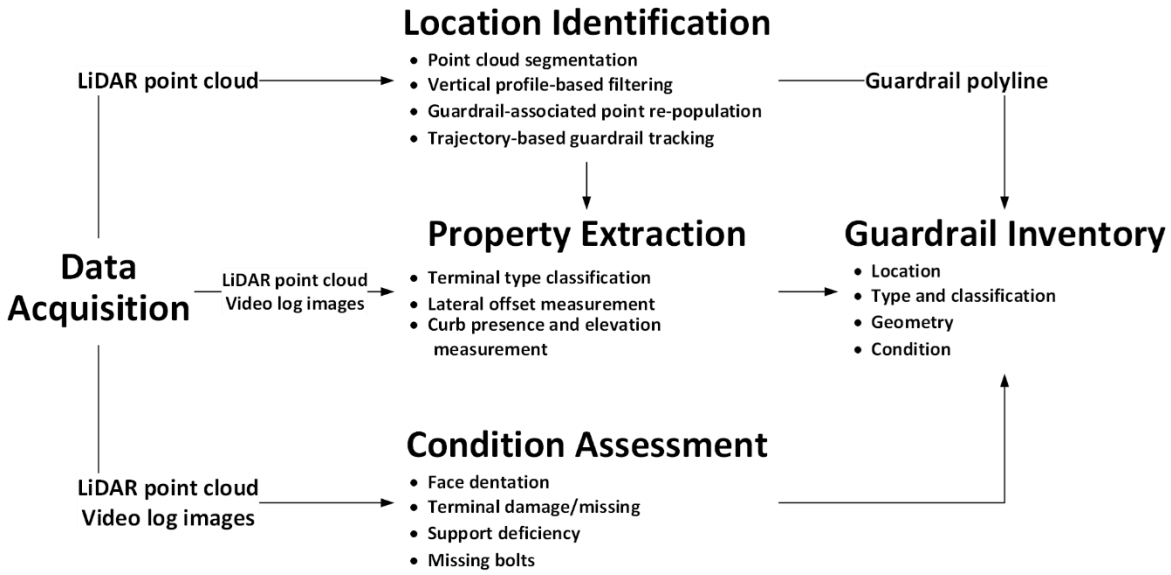


**Figure 2.1: Overview of data processing methodology**

## 2.2 Data Acquisition

The data acquisition system used in this study is an integrated mobile LiDAR system, RIEGL VMZ-2000, which consists of three primary components, including the LiDAR sensor, the precise positioning system, and the camera system. (Left: Overview; Middle: Camera and Mobile LiDAR; Right: Control panel)

Figure 2.2 shows the overview of the data acquisition system used in this study. The LiDAR sensor is used to acquire the point cloud of the roadway, including guardrails. Each point consists of the precise position information that is derived from the integrated precise positioning system. The integrated precise positioning system is used to acquire accurate coordinates that are composed of a global positioning system (GPS) and an inertial measurement unit (IMU). The camera system (FLIR Ladybug 5+ camera) is used to capture video log images that are registered to the LiDAR sensor. In this study, the point cloud data acquired by the LiDAR sensor was used for all the data processing steps, including location identification, property identification, and condition evaluation, while the video log images acquired by the camera system were used for property extraction and condition evaluation.

**The current LiDAR sensor can produce 400,000 measurements per second in both the line scanning mode and the radar scanning mode. For the application of the corridor scanning with the best point cloud density, the vertical line scanning mode was selected. (Left: Overview; Middle: Camera and Mobile LiDAR; Right: Control panel)**

Figure 2.2 shows the vertical configurations for the line scanning mode. For the vertical configuration, the scanning line of the LiDAR sensor is aligned perpendicular to the ground when the vehicle makes a longitudinal motion. The scanning line forms a 100° vertical fan to cover the road surface, especially the roadside objects. To acquire the point could with better homogeneity of point cloud densities, the frequency of the LiDAR sensor and the LiDAR heading angle were configured at 75 Hz (i.e., lines per second) and 135° (i.e., the angle to the vehicle driving direction), respectively.

**(Left: Overview; Middle: Camera and Mobile LiDAR; Right: Control panel)**

**Figure 2.2: Integrated data collection vehicle**

## 2.3 Guardrail Extraction using Mobile LiDAR

The objective of guardrail extraction is to identify the location of guardrails along the roadway by identifying their corresponding starting and ending points. This subsection presents the details of the developed guardrail extraction algorithm in this study, including a brief literature review (2.3.1) on previous research that is relevant to this study, the detailed descriptions of the features used for the algorithm development (2.3.2), an overview of the algorithm (2.3.3), and the newly developed point cloud segmentation, vertical profile-based filtering, point re-population, and the guardrail tracking methods (2.3.4-2.3.7).

### 2.3.1 Literature Review

Because of the criticality of the guardrail infrastructure, local transportation agencies invested their effort and resources in establishing the guardrail inventory for effective management, e.g., the Georgia Department of Transportation (GDOT) (*3*) and the Michigan Department of Transportation (MDOT) (*4*). Among these efforts, Vermont Agency of Transportation (*5*), the guardrail location information was collected in the field using hand-held global position system (GPS) data loggers or ArcGIS collector devices. Although detailed guardrail information could be collected using the field survey methods, it is extremely labor-intensive and time-consuming. Therefore, some agencies, e.g., Idaho Transportation Department (ITD) (*6*), used digital imaging data for inventory purposes that could provide the guardrail's location and other information (e.g., condition, etc.). While such a system provides better efficiency for data collection, some critical information, e.g., the geometry of guardrails, is challenging to acquire accurately. There remains a need for transportation agencies to employ an automated guardrail inventory method with efficiency and accuracy so that reliable guardrail information may be collected timely.

Research on automated guardrail detection is limited and mostly focuses on vision or radio detection and ranging (radar)-based approach. The preliminary guardrail detection research was conducted using vision-based methods (*3, 7*). For example, Seibert et al. (*8*) extracted the guardrail from the camera data using a texture-based area classification for localizing the border and a structure from motion to identify raised structures, e.g., the guardrail. Although these methods have good performances on guardrail detection, 3-D geometry measurement may be inaccurate due to camera calibration. As radar sensors can accurately capture near field geometry, radar-based data was employed in guardrail detection and condition extraction (*9–11*). Chipengo (*12*) proposed a novel guardrail system for high-pedestrian density areas based on the physical properties of guardrail radar returns. However, the moving vehicles may affect the accuracy of this approach (*13*). Some researchers attempted to fuse both vision and radar data (*14–16*) to achieve better robustness and accuracy. Among these studies, Alessandretti et al. (*17*) developed a vehicle and guardrail detection system

fusing radar and vision data, which extracted the region of interest for guardrails from the image and superimposed it on the radar data through cross-sensor registration. Although these methods (*14*, *17*) showed accurate results that may lead to a more efficient guardrail inventory practice compared to a manual survey in the field, the approach only works well at low speed because the errors of parameter measurement may occur when the extrinsic parameters change due to vehicle speed up, or road roughness.

With the popularity and affordability of the LiDAR sensor, there is an increasing number of successful applications of the point cloud data in roadway and roadside object extraction, e.g., cars (*18*), trains (*19*), pedestrians (*20*), traffic sign (*21*), pavement marking (*22*), sidewalk (*23*), curb (*24*), etc. These methods took advantage of several uniquely distinguishable features of the objects, such as shapes, e.g., plane and edges, photometry responses, e.g., reflectance and retroreflectivity, and geometrical measurements. e.g., length, width, and continuity of the objects. However, research using LiDAR point cloud for guardrail inventory has been limited. Zhu and Guo (*25*) proposed a beam guardrail detection algorithm containing feature extraction based on height feature and corner feature, and clustering steps in LiDAR data. Jiang et al. (*26*) developed a corrugated beam guardrail detection method based on guardrail sweeps, which contain bounding box, corner count, and height features, in mobile laser scanning data. These methods shared a similar processing pipeline that included the segmentation of the point cloud data into lines sequence and then extracted guardrail points based on an approximate two-dimensional (2-D) view. However, the limitations of these methods were evident as they could not accurately capture the local 3-D features of the guardrail that were overly simplified as line-based features during the segmentation. To overcome such a drawback, guardrail blocks were extracted based on the clustering outcome, e.g., density-based spatial clustering of applications with noise (DBSCAN). Gao et al. (*27*) proposed a rapid extraction approach for urban road guardrails using a multi-level filter with a modified DBSCAN clustering based on the subsampling point cloud. This approach achieves a good precision of 96.8% for two types of guardrails. However, not whole guardrail points are captured by this approach due to the processing step – subsampling, so some of the local features may be missing. Vidal et al. (*28*) proposed a guardrail and barrier extraction and classification method based on their geometry using Region of Interest (ROI) and DBSCAN. Although this parameter-dependent method has better results than other methods since the geometrical parameters can be predefined based on the norms in the specific road, it still has a lot of work to do when being implemented on different types of roads.

In summary, the automated guardrail extraction methods have been limited. While some attempts have been made using imaging and radar sensors, the performance remained to be improved due to the limited accuracy of image-based detection and radar-based measurements. Although others attempted to employ LiDAR point cloud for better guardrail detection with promising results, two challenges remain in the existing methods, especially

for a network-level application: 1) Although the current methods used partial local geometrical guardrail features, it is still a task to fully consider these 3-D local geometry features to enhance the accuracy; 2) Most of the current methods focus on a road or a segment of the road, it still has lots of further work to be implemented in the network-level roads for the transportation infrastructure inventory purpose.

### 2.3.2 3-D local features of guardrail

The 3-D local features of the guardrail (as shown in Figure 2.3) include four types of features: corrugation feature, vertical profile feature, connectivity feature, and continuity feature. The details of four types of features are described as follows:

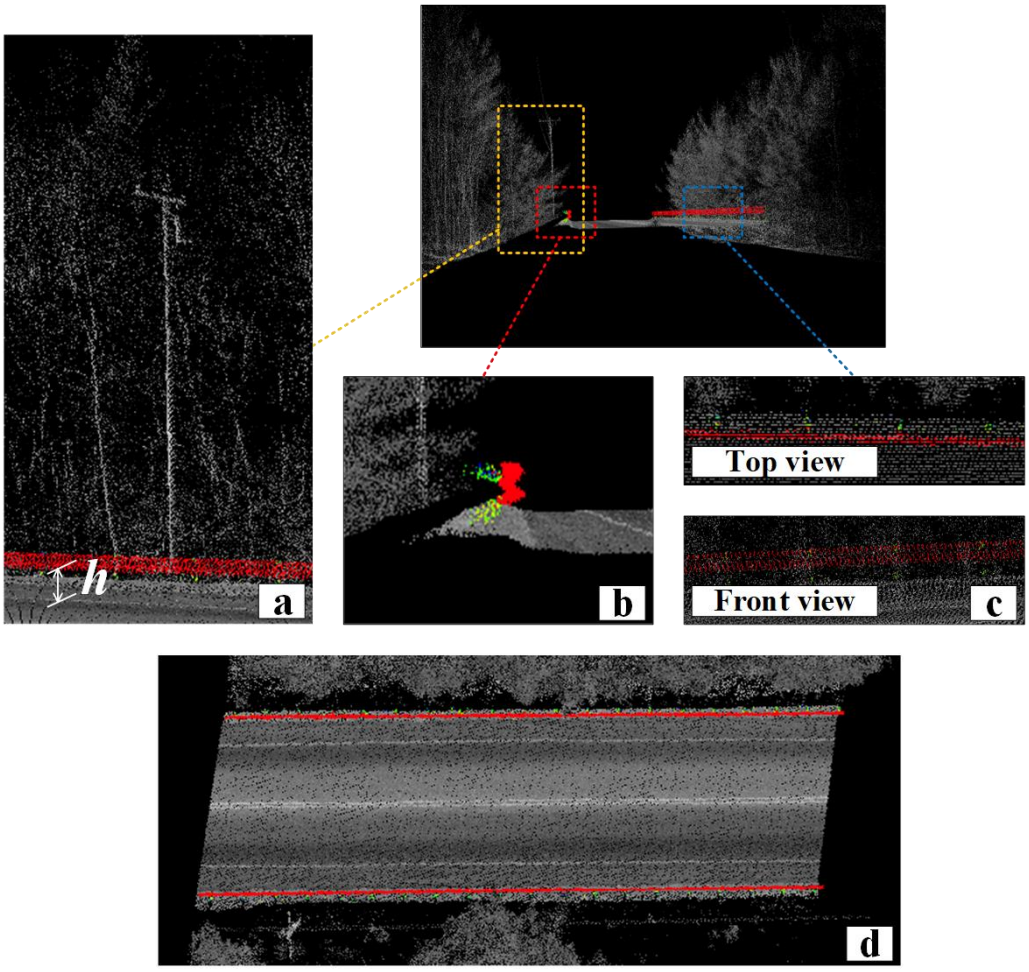


**Figure 2.3: Examples of 3-D local guardrail features**

- *Corrugation feature*: Surface corrugation of the guardrail is, by design, a critical safety feature to absorb impact energy to reduce the caused damage (*29*). Meanwhile, corrugation also renders a unique 3-D local feature that is visible in the point cloud. The vertical surface corrugation of the guardrail beams can be visually distinguished by the periodical, uneven surface compared to other common roadway and roadside objects,

which either renders a local, co-planer feature, pavements, or forms randomly distorted surfaces, e.g., vegetation, pedestrians, etc. As captured in the point cloud (shown in Figure 2.3(b)), such a periodical pattern of the guardrail's surface corrugation can be modeled based on the change of directions of the local surface normal vectors. These graduate changes of directions can be potentially used to distinguish guardrails from roadway objects with flat surfaces (e.g., pavements, sidewalks, etc.) whose normal directions remain the same and from other roadway and roadside objects with randomly distorted surfaces (e.g., vegetation, pedestrians, etc.) whose normal directions change significantly.

- *Vertical profile feature*: Vertical profile feature (as shown in Figure 2.3(a)) includes height and local profile feature. The height feature of the guardrail is the installation height regulated and standardized by local construction directives and norms. These directives and standards could provide the minimum and maximum height requirements. As a result, the guardrail has a different height from low-height objects, e.g., curbs, etc., and high-height objects, e.g., traffic signs, trees, etc. Besides, for the local profile feature, because of the variant point cloud density caused by the corrugated shape, the beam points have a bimodal height distribution that is different from others (e.g., curb, traffic sign pole, tree trunk, etc.), that have unimodal height distributions.
- *Connectivity feature*: The connectivity feature dictates the adjacency of the beam and spacer as well as the post, as shown in Figure 2.3(c). Since the point cloud structure is irregular and unorganized, the geometry connection of point-to-point is unique. The spacer and post points are closer to the beam points than other points belonging to non-guardrail objects, e.g., curbs, traffic signs, etc. The connectivity feature reflects the immediate connection between the beam points and the spacer points as well as the post points. The spacer and post can be extracted based on the connectivity feature and the outcome of beam detection.
- *Continuity feature*: The continuity feature is the longitudinal connectivity of the beam, as shown in Figure 2.3(d). The beams that are designed to install in some specific area to protect critical roadside properties, e.g., bridges, buildings, etc., from collisions are linearly distributed along the roadway. The beams have such significant continuity feature that is different from the discrete point-based distribution transportation infrastructures, e.g., traffic signs, parking meters, etc.

### 2.3.3 Method Overview

To leverage the four unique local features for guardrails captured in the point cloud data, including the corrugation feature, vertical profile feature, connectivity feature, and continuity feature, a fully automated algorithm is developed that consist of four corresponding steps: Difference of Normal (DoN)-based segmentation, vertical profile-based filtering, guardrail-associated point re-population, and guardrail tracking. The overview of the four-step is illustrated in Figure 2.4. While all four local features are used to identify guardrails in the

point cloud data, the proposed method tailors a processing sequence based on the significance and uniqueness of these features for better performance.

DoN-based segmentation is introduced first to extract the points that render the corrugation feature effectively. Then a vertical profile-based filtering process is applied to effectively remove the points with heights that are unlikely to follow the installation specification for guardrails and the points with consistent densities that are different from the variant density of the beam point cloud. The guardrail-associated point re-population is then utilized to reclaim the points associated with the spacer and post components of guardrails that are not always captured in their full forms. Finally, the extracted points are further tracked based on their positions (left and right-hand side of the road) and longitudinal adjacency.

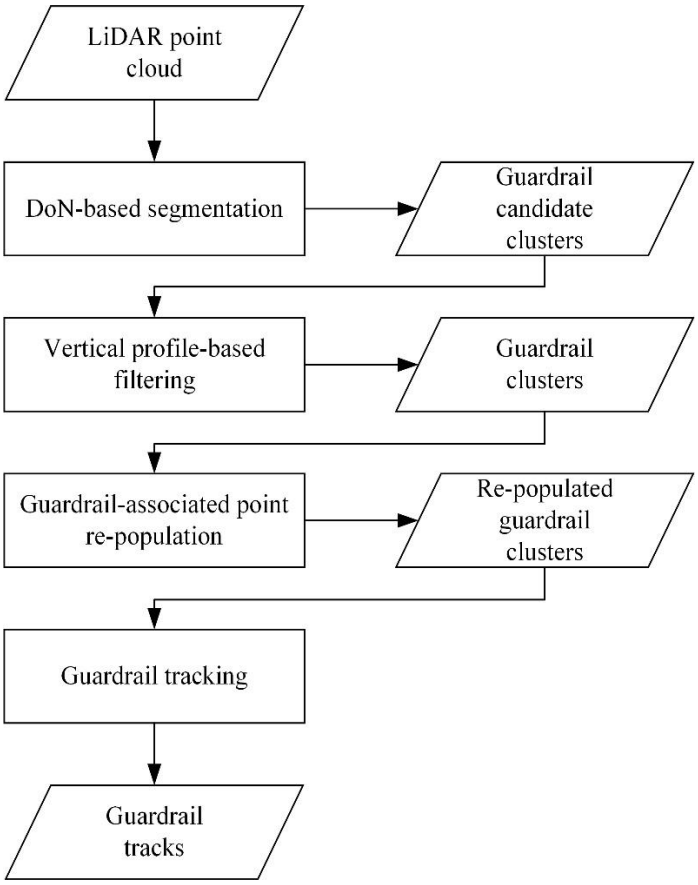


**Figure 2.4: Proposed automated guardrail extraction method**

### 2.3.4 DoN-based segmentation

DoN-based segmentation (*30*) takes full advantage of the corrugation feature of the guardrail surfaces. It deals with the non-planar surface of the unorganized point cloud by estimating the changes in the surface's normal directions in different local regions. Intuitively, in the flat regions of the point cloud, the normal directions of the regions do not vary, while in the corrugated regions of the point cloud, the normal directions for the regions significantly

change as the surface distorts. DoN is defined as the difference between two normal values estimated at two different scales (defined by a smaller radius and a larger radius) in the point cloud to capture such a phenomenon. The normal value evaluated at a given radius describes the underlying geometric properties (e.g., flatness, etc.) of the surface at the scale of the radius. Normal values evaluated with a large radius represent the geometry of the large-scale surface, while normal values evaluated with a small radius reflect the geometry of the local-level surface as well as noise. Consequently, the difference in the normal values at the two radii represents how much the local corrugation makes the local normal directions depart from the larger-scale flatness. There are no significant differences for the DoN values of the flat surfaces, e.g., pavement, sidewalk, etc., at different radii pairs, regardless two radii values are different or the same. The DoN values of the randomly distorted surfaces, e.g., vegetation, pedestrians, etc., change significantly at any radii pairs. As a unique feature, the DoN values of the corrugated surfaces of the guardrail change regularly at some radius pairs with a smaller radius and a larger radius. In this study, the DoN operator $\Delta_{\hat{n}}$ is introduced to estimate the surface geometry, defined as:

$$\boldsymbol{\Delta_{\hat{n}}(p, r_1, r_2) = \frac{\hat{n}(p, r_1) - \hat{n}(p, r_2)}{2}}$$

where $r_1, r_2 \in \mathbb{R}, r_1 < r_2$, and $\hat{n}(p, r)$ is the surface normal estimated at any point $p$, given the support radius $r$. The magnitude of the $\Delta_{\hat{n}}$ vector is always within [0,1] since each DoN is the normalized sum of two unit-normal vectors.

Four steps, which include DoN estimation, DoN-based filtering, plane removal, and Euclidean clustering, are designed to remove the objects with flat surfaces as well as randomly distorted surfaces and collect and cluster the guardrail candidate points in the DoN-based segmentation. Figure 2.5 shows the flowchart of the DoN-based segmentation method and the intermediate output corresponding to each step.

- *DoN estimation*: The surface normal values are estimated through Principal Component Analysis (PCA) with re-orienting normals based on a given viewpoint (*31*). Then, the DoN value of each point in the point cloud data is obtained through the estimated surface normal values as well as the equation above with the proper small and large radii pair. It should be noted that the selection for the radii pair is critical, as it defines the scales of the regions at which the corrugation feature can be revealed. The sensitivity study of the radii pair is presented in a later section.
- *DoN-based filtering*: Since the DoN values of the randomly distorted surfaces change significantly, this step is introduced to remove the objects (e.g., vegetation, etc.) with such surfaces based on the given DoN threshold (*30*). The point cloud data of the pavement and its surrounding infrastructures, e.g., guardrail and curb, etc., are collected from the filtered point cloud data.

- *Plane removal*: This step is utilized to remove the objects (e.g., pavement, sidewalk, etc.) with the flat surfaces through the Random sample consensus (RANSAC) method (*32*) from the outcomes of the DoN-based filtering. The flat surfaces are detected by fitting the plane model iteratively in the RANSAC method from the point cloud data.
- *Euclidean clustering*: The purpose of this step is to cluster the discrete points collected from the previous steps. Then these generated clusters through Euclidean clustering (*31*) could be used for the subsequent guardrail extraction steps. These generated clusters are parts of some objects, e.g., guardrails, sign poles, tree trunks, etc.

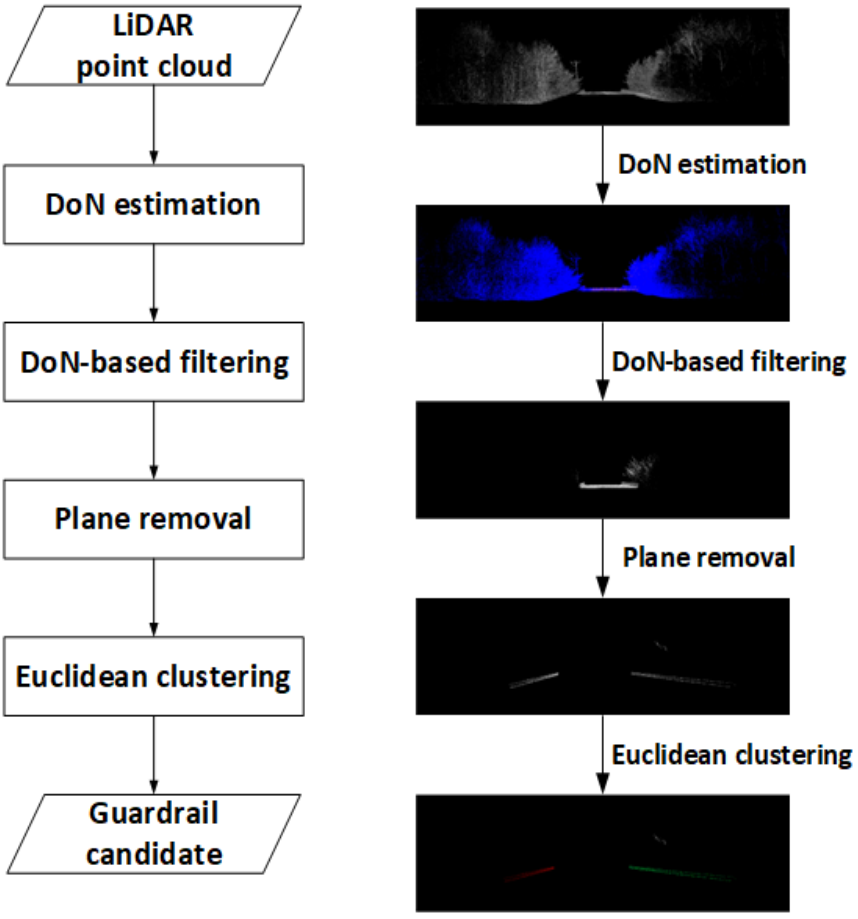


**Figure 2.5: Proposed DoN-based segmentation method**

### 2.3.5 Vertical profile-based filtering

After the DoN-based segmentation, the point cloud is segmented into clusters within which the points share similar DoN properties (e.g., corrugation surface). However, many noise clusters, e.g., curb, pavement, tree, etc., may also render similar properties to guardrail beams. Therefore, it is necessary to filter these candidate clusters further and retain those truly associated with guardrails. Since guardrails are installed at a specified height above the ground to ensure the best protection and prevention functionality as defined in the guardrail

installation manuals (*33*), the height feature can be used as a strong criterion to remove noise clusters. Besides, because of the variant density caused by the corrugated shape of the beam, this local profile feature is utilized to remove the noise clusters with consistent densities. The following two specific properties are introduced to robustly identify the vertical profile feature, including the height thresholds (to efficiently reject point cloud clusters that are located at an impossible height above the ground to be a guardrail) and the height distribution (to effectively reject point cloud clusters that may share similar heights as a guardrail, but have a wider spread of points along the vertical direction, e.g., walls, etc.).

- *Height Threshold*: The height threshold is defined as the average height of the candidate cluster above the ground. Therefore, the guardrail height thresholds are determined based on the requirements regulated and standardized by the installation specifications. For example, there is a minimum height requirement of 26.5 inches (0.673 m) for the W-beam guardrail defined in the installation specification, e.g., MassDOT Highway Division – Engineering Directive (*33*). The guardrail height maximum threshold $h_{tmax}$ and minimum threshold $h_{tmin}$ are defined as:

$$h_{tmax} = h_{max} - h_{cl}/2$$
$$h_{tmin} = h_{min} + h_{cl}/2$$

  where $h_{max}$ and $h_{min}$ are the maximum and minimum height requirements regulated by the local construction directives and norms. $h_{cl}$ is the minimum cross-section length requirement of the guardrail regulated by the local construction directives and norms.

  Combing through the heights of the centroids of the guardrail candidate clusters, the height thresholds are utilized to filter most noise clusters with higher heights, e.g., the pole of a traffic sign, tree trunk, etc., as well as others with lower heights, e.g., curb, etc.

  - *Removal of noise cluster with high height*: if $h_c > h_{tmax}$, the noise cluster with high height is removed.
  - *Removal of noise cluster with low height*: if $h_c < h_{tmin}$, the noise cluster with low height is removed.

  where $h_c$ is the height of the centroid of the guardrail candidate cluster.

- *Height Distribution*: The height distribution is defined as the height distribution of each point within the candidate cluster off the ground. Some noise objects, e.g., walls, bushes, etc., may share a similar average height as guardrails. The height distribution of their associated points in these clusters is significantly different from those associated with guardrail clusters. For a guardrail cluster, the height distribution of the points has a bimodal distribution, as shown in Figure 2.6(a), because of the sparse points caused by the corrugated shape. Few points contribute to the height numbers in the valley bottom of

the height distribution since the middle of the beam point cloud has a sparser density than the densities of the top and bottom parts caused by the corrugated shape. Different from the guardrail cluster, the noise cluster, e.g., wall, etc., has a unimodal height distribution (shown in Figure 2.6(b)) since it has a consistent density.

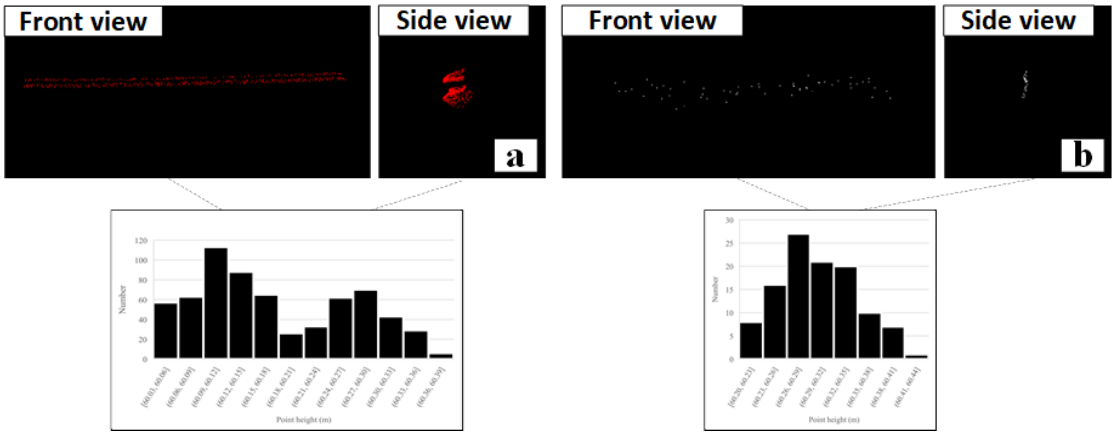


**Figure 2.6: Vertical profile and point clusters**

### 2.3.6 Guardrail-associated point re-population

Depending on the data collection configurations, guardrail beams are usually the predominant component captured in the point cloud, while guardrail spacers and posts can only be captured partially. However, it remains important not to exclude these important components from extraction, especially for supporting guardrail inventory purposes (e.g., condition evaluation). While independently identifying these components with incomplete shapes may be challenging, their immediate connectivity to guardrail beams can be leveraged to retrieve the associated points better. Therefore, a guardrail-associated point re-population step is introduced based on a voxel search on an octree structure of the point cloud (*34*). The basic idea of the re-population process is to seek the points that are associated with posts and spacers with the proximity of voxels defined in the octree data structure, and it relies on the condition that the majority of the guardrail-associated points, i.e., guardrail beam, has been extracted from previous steps.

The octree data structure is built in the original input point cloud data. The space is recursively subdivided into eight octants. Each final subspace is called a voxel (as shown in Figure 2.7). The voxel size is set based on the rule that this subspace includes as many ignored guardrail points in the previous step as possible, especially in the guardrail boundary area. If the voxel size is too large, interfering point data will be re-populated; otherwise, many points associated with post and spacers will be missed. The voxel size represents the search buffer around the extracted guardrail beam-associated points (seed points). Given the voxel size's criticality, the voxel size's sensitivity was also analyzed (in the later section). In each voxel, the neighbor points (blue points as shown in Figure 2.7) of each extracted point

that is associated with guardrail beams (red points as shown in Figure 2.7) in the extracted guardrail cluster are searched based on the original input point cloud data. If any points (green points as shown in Figure 2.7) are not within the voxels containing guardrail beam points, they are not extracted as guardrail-associated points. The re-population process will not be complete until all the seed points are visited. Some points may be retrieved multiple times in the voxel search (single voxel shown in Figure 2.7). These duplicate points are removed based on their 3-D coordinate values.

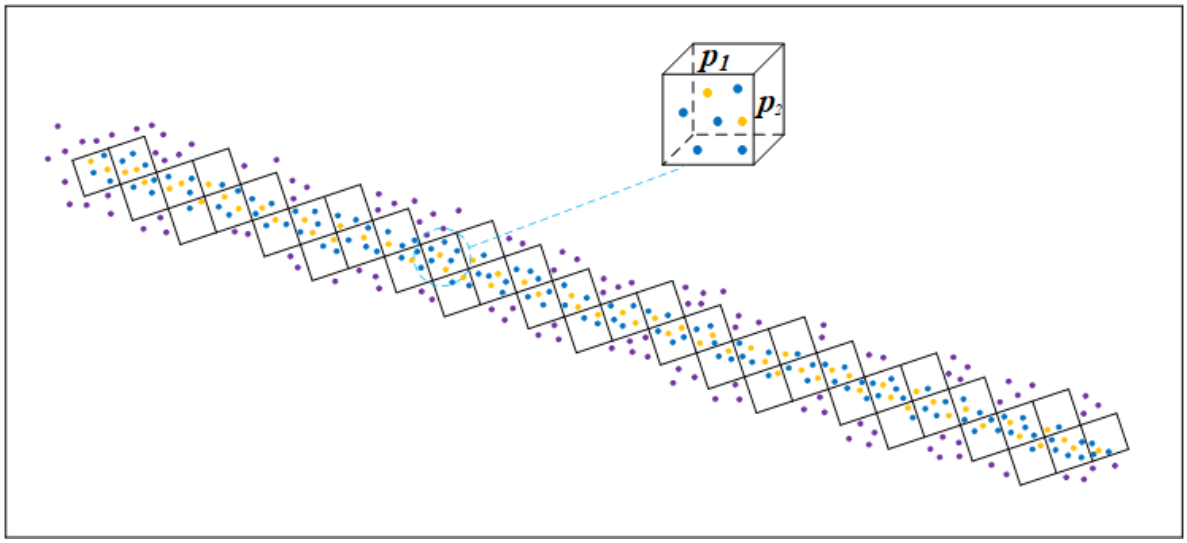


**Figure 2.7: Voxel search on octree structure**

### 2.3.7 Guardrail tracking

The objective of the guardrail tracking step is to find the complete track of the guardrail based on the continuity feature of the guardrail. Guardrail tracking includes two sub-steps, including 1) guardrail position identification and 2) guardrail continuity determination (as shown in Figure 2.8(a) and (b), respectively). The vehicle trajectory is introduced to aid two steps since the guardrails are distributed along the roadway. The assumption of the vehicle trajectory holds true as LiDAR point cloud data is always captured with its corresponding vehicle trajectories. Therefore, this step uses the vehicle trajectory data. However, for any point cloud data without vehicle trajectories, similar information may be extracted from pavement marking information along the road, and the following steps remain valid.

The positions (i.e., left/right side of the road) of the extracted guardrail-associated clusters need to be identified. An algorithm based on the cross-product of the vehicle trajectory and the extracted guardrail-associated point clusters (*35*) is introduced to determine the positions. For the 2-D vehicle trajectory and guardrail cluster that are projected into the horizontal plane ($xoy$ plane in the Cartesian coordinate system), there are two random points $A(x_1, y_1)$ and $B(x_2, y_2)$ in the 2-D vehicle trajectory and one random point $P(x_0, y_0)$ in the guardrail cluster (as shown in Figure 2.8(a)). Then, the position of point $P$ based on the signed line $AB$

from $A$ to $B$. There are two vectors $\overrightarrow{AB}(x_2 - x_1, y_2 - y_1)$ and $\overrightarrow{AP}(x_0 - x_1, y_0 - y_1)$. The cross product of $\overrightarrow{AB} \times \overrightarrow{AP}$ is defined as,

$$\overrightarrow{AB} \times \overrightarrow{AP} = \left|\overrightarrow{AB}\right|\left|\overrightarrow{AP}\right|\sin\varphi$$

where $\varphi$ is the angle between $\overrightarrow{AB}$ and $\overrightarrow{AP}$.

The position of $P$ depends on $\overrightarrow{AB} \times \overrightarrow{AP}$ when $\left|\overrightarrow{AB}\right|\left|\overrightarrow{AP}\right| \neq 0$. Geometrically, the position of $P$ depends on the $z$-component of $\overrightarrow{AB} \times \overrightarrow{AP}$ based on the right-hand rule. Consequently, the identification rule is as follows,

- *Left side*: If $(x_2 - x_1)(y_0 - y_1) - (y_2 - y_1)(x_0 - x_1) > 0$, $P$ is on the left side of the signed line $AB$. The guardrail cluster is on the left side of the road accordingly.
- *Right side*: If $(x_2 - x_1)(y_0 - y_1) - (y_2 - y_1)(x_0 - x_1) < 0$, $P$ is on the right side of the signed line $AB$. The guardrail cluster is on the right side of the road accordingly.

The steps mentioned above will be robustly extracted guardrail-associated points. Unfortunately, due to the nature of the LiDAR point cloud data collection, occlusion that blocks the line of sights, e.g., cars, may frequently occur and can artificially break the continuity of guardrails captured in the data. Therefore, the guardrail clusters, if broken, need to be connected into one guardrail section. A guardrail continuity determination rule is proposed in this study. The guardrail points are projected into the vehicle trajectory based on a linear reference system (*36*), as shown in Figure 2.8(b). The guardrail position (the left/right side of the road) is identified through the proposed guardrail position identification method. Then, the whole guardrail cluster is projected into new guardrail clusters along the vehicle trajectory. On the same side, two neighboring clusters will be connected as the same guardrail if the distance $d_{i,j}$ between the closest point pair, i.e., $P_{pi}$ of projected cluster $i$ and $P_{pj}$ of the projected cluster $j$ is within a distance threshold $\Delta_d$, which can be set as the maximum occlusion that may occur during the data collection. In this study, 9.0m (6.56 ft) is used as $\Delta_d$ based on the double average car length.

- *Same guardrail*: if $d_{i,j} \leq \Delta_d$, two clusters belong to the same guardrail.
- *Different guardrails*: if $d_{i,j} > \Delta_d$, two clusters belong to different guardrails.

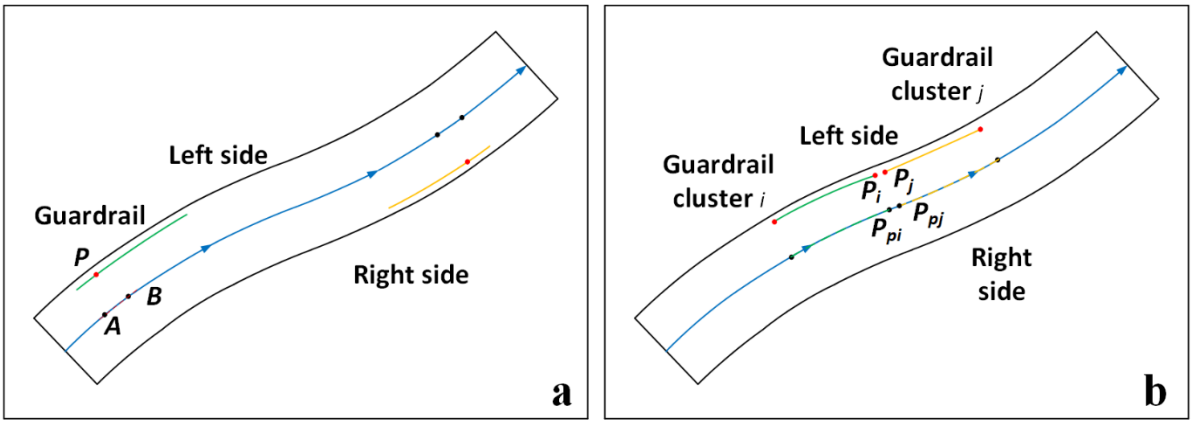


**Figure 2.8: Guardrail tracking—2-D profiles**

## 2.4 Guardrail Property Identification using Mobile LiDAR and Image Processing

The objective of guardrail property extraction is to identify detailed properties of the extracted guardrail, including guardrail type (e.g., terminal and beam types) and geometry information (e.g., curb presence, guardrail elevation, and lateral offset). This subsection presents the details of the developed guardrail property identification algorithm in this study, including a brief literature review (2.4.1) on previous research that is relevant to this study, an overview of the algorithm (2.4.2), and the newly developed terminal and beam type identification algorithms and the geometry measurement methods (2.4.3 and 2.4.4, respectively).

### 2.4.1 Literature Review

In the MASH (*2*), the guardrail inventory should include the location and design details of the installations so that the information can be matched to the crash data for evaluation. For the design details of the guardrail installations, the National Cooperative Highway Research Program (NCHRP) Report 490 - In-Service Performance of Traffic Barriers (*37*) provides the installation characteristics, including length, post numbering, post spacing, rail height, lateral offset, nearest hazard, side slopes, hardware description, lane and shoulder widths, horizontal and vertical curvature, and special features, etc. In this study, the proposed method mainly focuses on the location and some of these characteristics, including the length, height, offset, etc. Other guardrail installation characteristics will be considered in further research.

The current guardrail inventory conducted by the local agencies collected limited guardrail geometric parameters. Some spatial information (e.g., height, lateral offset, etc.) is always inaccurate or missing by either using the estimated field measurements due to the unsafe

operation on-site or leveraging video log imagery and GIS due to the incomplete data type. Therefore, in this study, the proposed automated geometry measurement method can provide not only the required parameters, e.g., guardrail location, height, length, and lateral offset (from the edge of the pavement to the guardrail), but also other parameters, e.g., cross-section height, etc. This 3D geometric information could be utilized for different purposes, e.g., asset management, maintenance, and safety analysis.

### 2.4.2 Method Overview

Properties of guardrails are critical to their functionality and efficacy. The objective of this guardrail property identification method is to extract these critical properties by leveraging the results for the extracted guardrails from the previous step (as presented in 2.3) and the additional rich information from the collected data from the LiDAR and camera systems. In this study, two categories of properties were concentrated, including the terminal type of the guardrail and the geometrical measurements of the guardrail. Figure 2.9 shows the overview of the proposed method for extracting these critical guardrail properties.

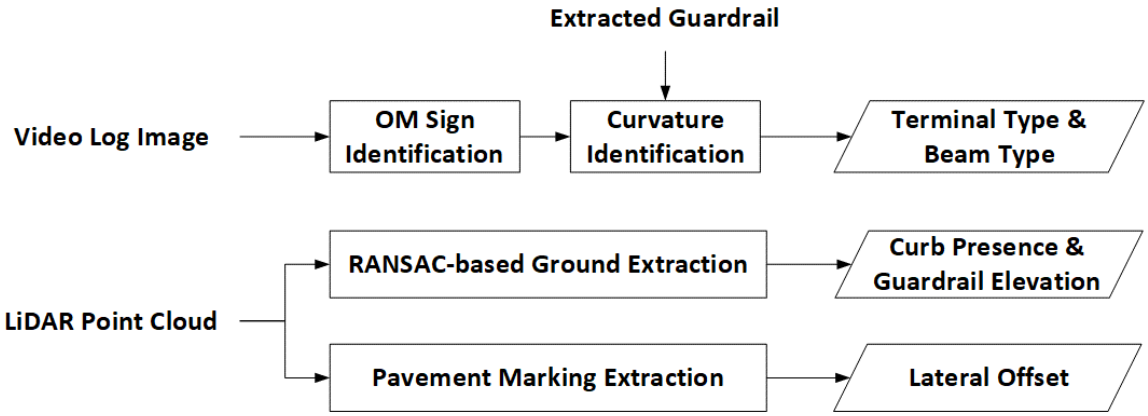


**Figure 2.9: Overview— proposed guardrail property extraction**

### 2.4.3 Guardrail Terminal Type Identification

A guardrail terminal (also called end treatment) refers to the starting point of the guardrail that is designed to clearly mark the delineation of the installed guardrail and is a critical component for absorbing energy if any impacts occur. Figure 2.10 shows examples of the guardrail terminals that are documented in the FHWA roadside terminal list for their frequent use in the field (*38*). Although some of the designs do not meet the criteria of different testing protocols, e.g., NCHRP 350, MASH, etc., unfortunately, they are still in service in the field due to the backlog of a complete inventory. It can be observed that, with different required performance characteristics and in compliance with testing protocols, the design characteristics, materials, and structures of guardrail terminals vary significantly. As identified in the literature review, few attempts have been made to automate the process due to such a challenge. In this study, the research team aimed at two general yet significant

features that are universally applied to most terminal designs, including the object markers (i.e., OM sign) and the bending curvature of the terminal, except for the buried-in-backslope (BIB) terminal design. Therefore, to identify the clearance markers, the research team introduced a high-performance traffic sign detection method developed by Tsai et al. (*39*) that has been validated in the implementation of interstate sign inventory efforts by the GDOT. To identify the bending curvature of the terminal, the research team introduced a surface normal variance criterion for classifying different types.


**Figure 2.10: Guardrail terminal shapes**

*2.4.3.1 OM Sign Identification*

The objective of the OM sign identification algorithm is to identify the region of the possible guardrail terminals in the collected video log images and then cross-referenced to the extracted guardrail location from the LiDAR point cloud data so that the corresponding point cloud clusters associated with guardrail terminals can then be extracted for the subsequent terminal classification algorithm. It should be noted that the mobile LiDAR system and the camera system have already been calibrated by the vendor (i.e., RIEGL), which means that each point from the LiDAR point cloud has a unique projection to an image pixel from the video log image.

Therefore, the cross-referencing process only requires a direct projection between the extracted guardrail region from the 3D point cloud to the video log image. Figure 2.11,

adopted from (*40*), shows an illustration of the projection process (where A represents a point within the point cloud, and the Earth-Center Earth-Fixed (ECEF) reference system refers to the Massachusetts state plane in this study). If an OM sign is identified within the projected region in the video log image, the points that are associated with the regions of the detected OM sign are extracted for the subsequent terminal classification algorithm. If no OM signs are identified within the project region in the video log image, a BIB terminal or a missing terminal type is assigned to the extracted guardrail.

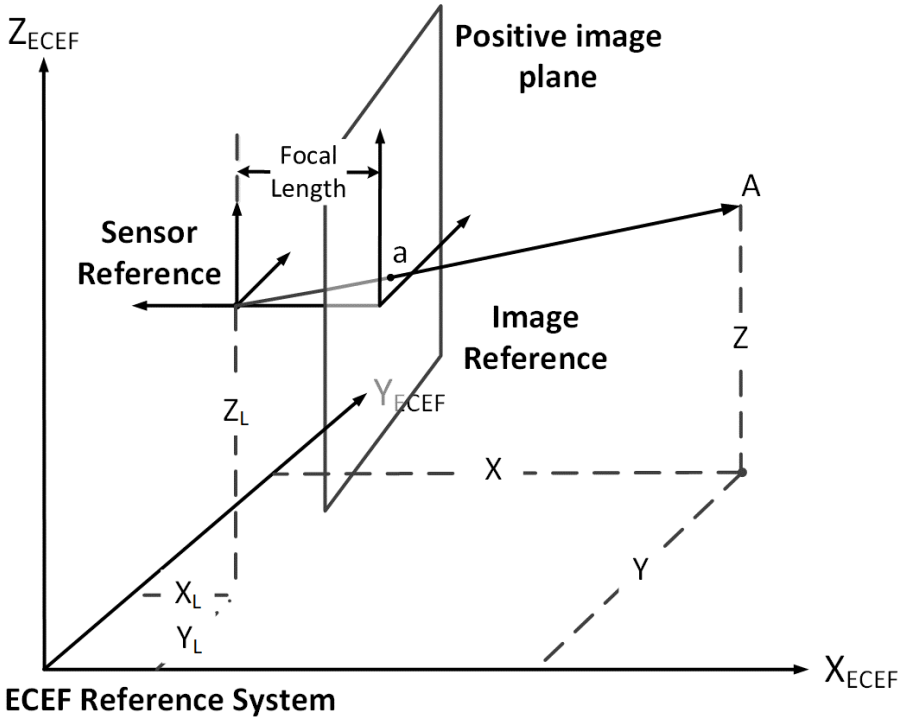


**Figure 2.11: Projection process: camera system and LiDAR point cloud**

In this study, the traffic sign detection method developed by Ai and Tsai (*41*) was applied to automatically extract regions of interest (ROIs) for the OM sign from video log images. The developed algorithm can achieve a detection rate of more than 85% for all types of traffic signs under different roadway conditions. Thanks to the unique pattern and color of the OM sign and the need for processing only a smaller region of the video image, a detection rate of more than 95% was achieved in this study. To achieve full coverage of OM signs, manual intervention is needed to identify the remaining approximately 5% of the undetected traffic signs, which are often associated with signs with faded color or damaged surfaces.

*2.4.3.2 Curvature Identification*

The objective of the curvature identification algorithm is to identify the degree of the surface bending at a guardrail terminal. By distinguishing the degree of bending, different types of guardrail terminals can be classified. As shown in the bounding boxes in Figure 2.12, there are

three types of bending patterns that exist in the in-service guardrails, including the curved surface (circular bending), the flat surface (no bending), and the buried surface (i.e., BIB terminal only). As the BIB terminal has already been identified from the OM sign detection step, this curvature identification algorithm focuses on distinguishing the curved and flat surfaces.

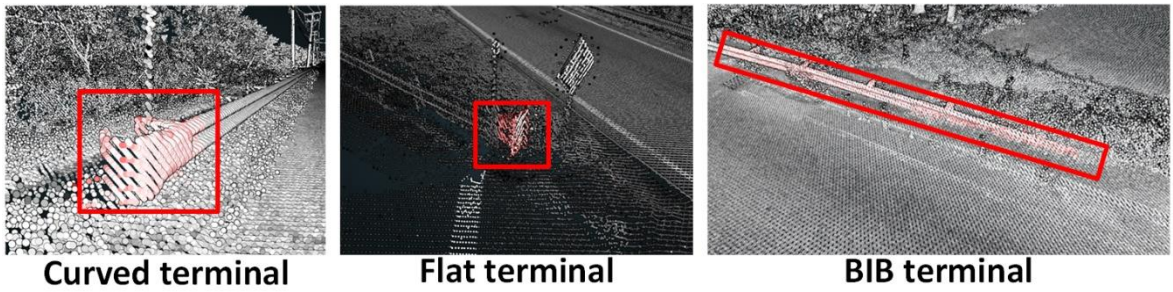


**Figure 2.12: Bending patterns of guardrail terminals**

As shown in Figure 2.12, the small clusters of points are distributed along the surface of the corresponding guardrails, which renders the curved, flat, and special surfaces, respectively. For the curved surface, the normal directions of its associated points will point toward different directions that trace the curved surface, whereas, for the flat surface, the normal directions of its associated points will point toward a single direction that is perpendicular to the flat surface. Therefore, the curvature identification algorithm is developed by computing the normal directions of the LiDAR points that are associated with the extracted terminal and then by summarizing the distribution of the computed normal directions.

For each point $x$ in the point cloud, $k$ nearest neighbors $x_i$ (i.e., all the points within a ball volume defined by the distance $r$) of the point $x$ are selected $x_i | \|x_i - x\| < r$. To compute the local normal of the point $x$, a plane $p_i$ is identified that minimizes the sum of square distances between all the points within the set $x_i$ and the plane $p_i$.

$$min \sum_{i=1}^{n} dist(x_i, \pi)^2$$

In this study, the plane is identified using a local plane fitting method through principal component analysis (PCA) (*42*). The PCA computation is applied to every point within the point cloud that is within the guardrail terminal cluster. Therefore, a distribution of local normal directions is derived for each terminal-associated cluster. If the distribution of the computed normal directions shows a "uniform pattern," a curved surface is identified; if the distribution of the computed normal directions shows a "single peak pattern," a flat surface is identified. In this study, the subcategories of guardrail terminals defined by FHWA and AASHTO (*38*) were not further explored due to the limited data samples. However, the

proposed curvature identification algorithm is general enough to be applied to other types of guardrails.

In addition to the terminal type, the identification of beam types was also explored based on the curvature of the surface along with the vertical profile of the guardrail beam, using the same PCA approach. Instead of identifying the distribution of normal from the point cloud that is associated with the guardrail surface, the distributions of normal were computed from the point cloud that is associated with a short section of the guardrail beam. In this study, w-beam, thrie-beam, double w-beam, and double thrie-beam were distinguished.

### 2.4.4 Guardrail Geometry Measurement

The current guardrail inventory conducted by the local agencies collected limited guardrail geometry parameters. Some spatial information (e.g., height, lateral offset, etc.) is always inaccurate or missing by either using the estimated field measurements due to the unsafe operation on-site or leveraging video log imagery and GIS due to the incomplete data type. Therefore, in this study, the proposed automated geometry measurement method can provide not only the required parameters, e.g., guardrail location, height, length, and lateral offset (from the edge of the pavement to the guardrail), but also other parameters, e.g., cross-section height, etc. This 3D geometric information could be utilized for different purposes, e.g., asset management, maintenance, and safety analysis. Figure 2.13 shows the details of how these geometry properties are defined in this study.

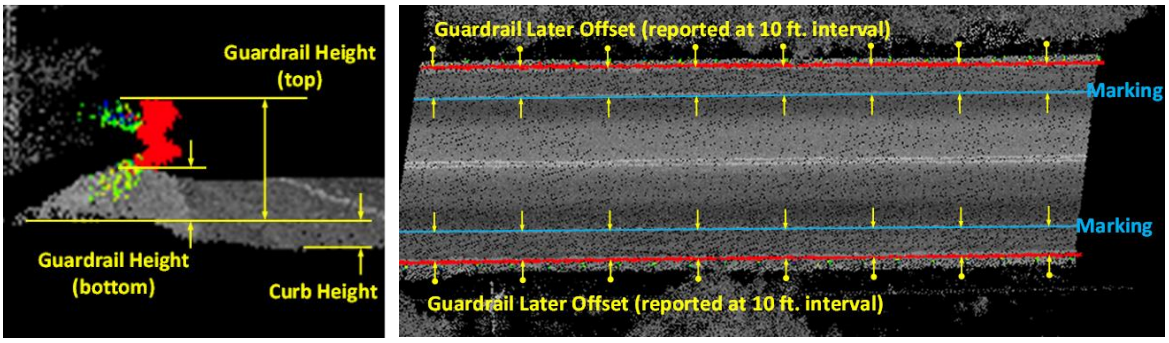


**Figure 2.13: Guardrail geometry properties**

The proposed automated geometry measurement method includes the following steps:

- *Guardrail boundary detection*: the boundary points of the guardrail beam can be identified by comparing the angles of the query point $p_q$ and its neighbors in a given radius area (Rusu 2009). $p_q$ is identified as the boundary point, defined as

$$\max\left(\alpha = \theta_{i+1} - \theta_i\right) \geq \alpha_{th}$$

where $\theta_{i+1}$ and $\theta_i$ are the angles between the lines formed by the points $p_{i+1}$ and $p_i$ in the neighborhood with $p_q$; $\alpha_{th}$ is the maximum given threshold angle, with a value of $\pi/2$ giving good results in most cases. The extracted guardrail boundary points are subsequently used for conducting the measurement of the guardrail's dimensions.

- *Guardrail location identification*: the location can be identified based on the georeferenced starting and ending points. The delineation of the guardrail is then determined by the distance of the two extreme vertical boundaries derived from the extracted guardrail boundary points. The details of the guardrail identification process have been presented in Subsection 2.3.
- *Guardrail length measurement*: the length represents the length of the covered section along the roadway; it is defined by the total length of the guardrail that is projected into the roadway. The guardrail length is measured based on the guardrail beam boundary points. All the beam boundary points are projected into the vehicle GPS trajectory in the $xoy$ plane, Cartesian coordinate system (Beam projected points in the vehicle GPS trajectory, as shown in Figure 2.14(a). The length $L_i$ is the total accumulation of the single Euclidean distance $l_i$ of two neighboring points, which are projected into the vehicle's GPS trajectory.

$$L_i = \sum_{i=1}^{n} l_i$$

- *Guardrail cross-section height measurement*: the guardrail cross-section height is a set of all the single height $h_i^{cs}$, that is, the Euclidean distance of each lower beam boundary point and its corresponding nearest upper beam boundary point (as shown in Figure 2.14 (c)).
- *Guardrail height measurement*: the height is the vertical distance from the top of the beam to the paved or unpaved surface below the guardrail. In this study, the guardrail height from the beam top to the ground surface is a set of all the single height $h_i^g$, as shown in Figure 2.14(d), that is the nearest Euclidean distance of each upper beam boundary point and the estimated plane of the ground surface extracted using the RANSAC-based method (*43*). If the curb exists, the guardrail height from the beam top to the curb top is a set of all the single height $h_i^c$, as shown in Figure 2.14(d), that is the nearest Euclidean distance of each upper beam boundary point and the estimated plane of the curb top extracted through the elevation-based method (*44*).
- *Guardrail lateral offset measurement*: both the upper and lower boundary points are projected into the horizontal plane (*x-o-y* plane) in the Cartesian coordinate system. Then, these boundary points are merged if the boundary points are in the same square. The square size is selected based on the mean distance of these points. The lower projected boundary points are chosen if the upper and lower projected points if these points are in

the same square. The guardrail's lateral offset is a set of all single lateral offset $l_i^{lo}$, that is, the Euclidean distance of each merged boundary point in the $xoy$ plane and its corresponding nearest point in the road boundary that is extracted by combining the intensity-based method (*45*) from the ground-level point cloud data (as shown in Figure 2.14 (b)) through RANSAC-based extraction (*43*).

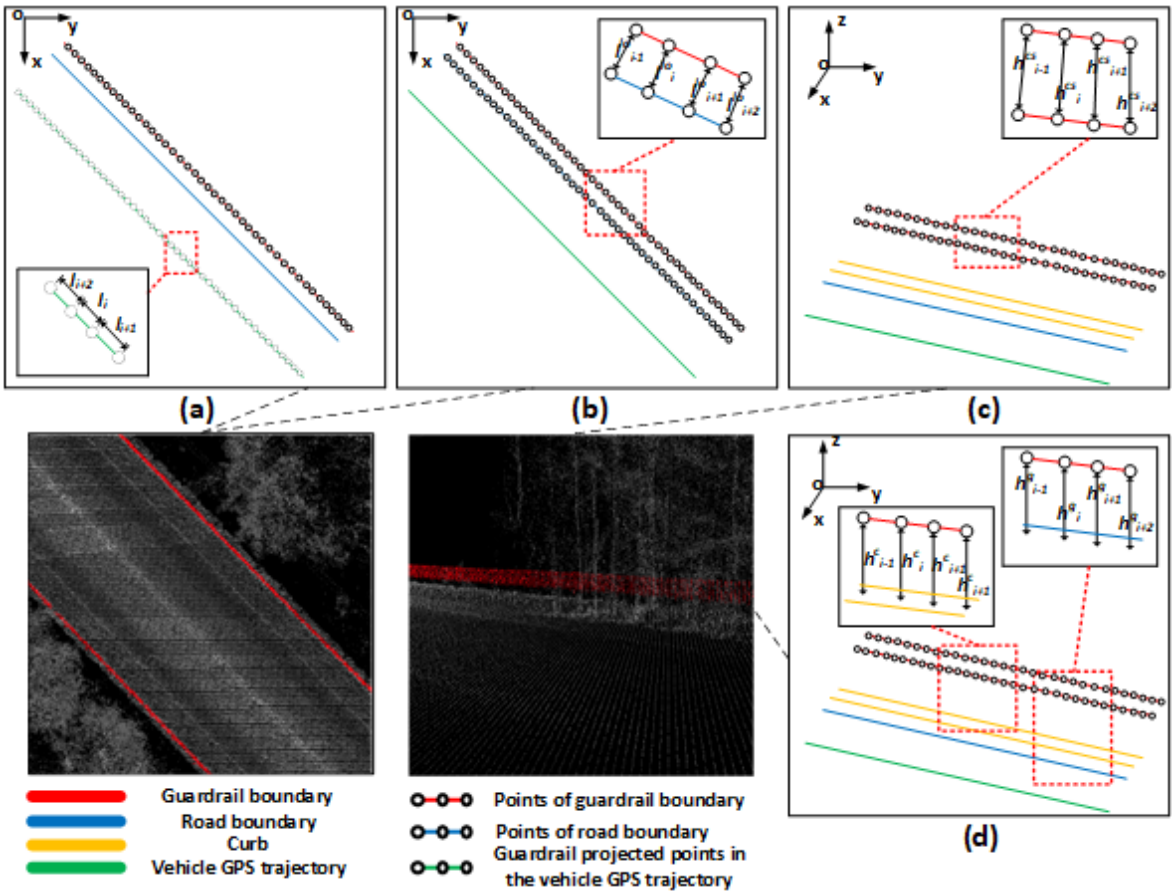


**Figure 2.14: Automated geometry measurement method**

The guardrail, consisting of a large, consistent, and linear beam, can be measured based on the same interval for the length $L_i$, cross-section height $H_i^{cs}$, height $H_i$, lateral offset $L_i^{lo}$, depending on the specific situations. The length $L$, average cross-section height $H_a^{cs}$, average height $H_a$, average lateral offset $L_a^{lo}$ are calculated based on $L_i$, $H_i^{cs}$, $H_i\$$ and $L_i^{lo}$ of $n$ subsections, defined as,

$$\begin{cases} \mathrm{L} = \sum_{i=1}^{n} L_i \\ H_a^{cs} = \dfrac{\sum_{i=1}^{n} H_i^{cs}}{n} \\ H_a = \dfrac{\sum_{i=1}^{n} H_i}{n} \\ L_a^{lo} = \dfrac{\sum_{i=1}^{n} L_i^{lo}}{n} \end{cases}$$

## 2.5 Guardrail Condition Assessment using Point Cloud and Computer Vision

The objective of guardrail condition assessment is to identify detailed conditions of the extracted guardrail, including face dentation, end terminal damage or missing, and guardrail support deficiency. This subsection presents the details of the developed guardrail condition assessment algorithms in this study, including a brief literature review (2.5.1) on previous research that is relevant to this study, an overview of the algorithm (2.5.2), and the newly developed condition assessment algorithms for face dentation (2.5.3), end terminal damage or missing terminals (2.5.4), support deficiency (2.5.5) and the exploration of missing bolt identification (2.5.6).

### 2.5.1 Literature Review

The research team did not find any previous literature that is directly relevant to automated methods for assessing guardrail conditions. Instead, some practical guidelines and processes for field inspection have been identified. For metal beam barrier rail elements, some quantitative repair criteria (*46*), including barrier deflection, damage to posts, post deflection, missing bolts, etc., are used by the transportation agencies. Most agencies use barrier deflection, the most prevalent quantitative repair criterion, with the FHWA-endorsed 6-inch threshold (*47*, *48*). One or more broken or cracked posts are the thresholds for the damage to posts by most agencies. For post deflection, most agencies inspect longitudinal distances that are out of alignment, while Pennsylvania uses post angle (*49*). For metal beam barrier connections, most maintenance assessment criteria rate a barrier as deficient if one or more bolts are missing, but none of the quantitative maintenance criteria use a threshold for missing bolts (*46*).

### 2.5.2 Method Overview

Deteriorated and damaged guardrails will significantly affect the durability and the original functionality of these critical safety assets. The condition assessment method developed in

this study is to identify several conditions by leveraging the results for the extracted guardrails from the previous steps (as presented in 2.3) and the additional rich information from the collected data from the LiDAR and camera systems. In this study, several algorithms were developed to automatically identify the conditions of guardrails, including face dentation, damaged and missing terminal, and deficient support. In addition, the feasibility of identifying missing bolts through video log images was also explored. Figure 2.15 shows the overview of the proposed method for assessing these critical conditions.

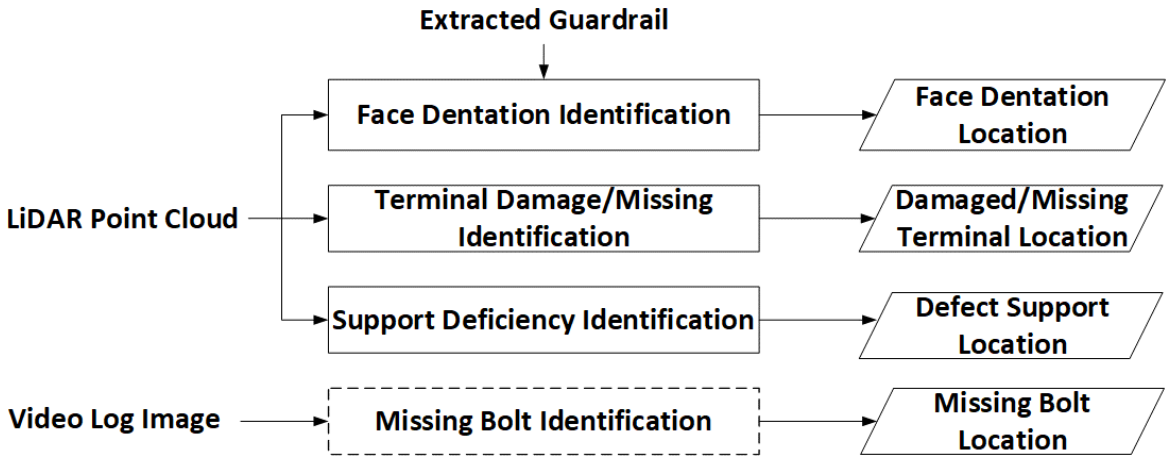


**Figure 2.15: Proposed guardrail condition assessment method**

### 2.5.3 Face Dentation Identification

The objective of the developed face dentation identification algorithm is to automatically identify the beam distortion, often caused by direction crash impacts. Figure 2.16 (bounding boxes) shows an example of face dentation as shown in the LiDAR point cloud data and the corresponding video log image data. It can be observed that the dentation partially flattens the surface so that the original wave pattern (e.g., W-shape and thrie-shape) of the guardrail beam is no longer present. To automatically identify these dentations along the extracted guardrails and quantify their distortion, the developed algorithm introduces a two-step processing for investigating the longitudinal profile of the guardrail and for investigating the vertical profile, respectively.

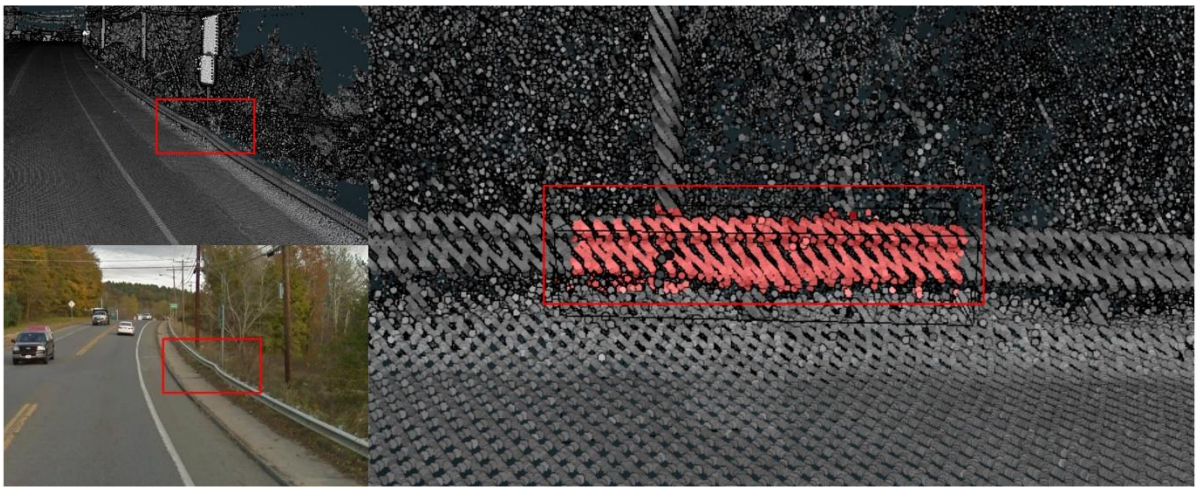

**Figure 2.16: Face dentation—LiDAR and a video log image**

- *Longitudinal Profile Evaluation*: For each extracted guardrail (as presented in Subsection 2.3), the lateral offset measurement (as presented in Subsection 2.4) is reconducted to generate the longitudinal profile. When a face dentation is observed, the longitudinal profile often demonstrates a local, outward distortion. More importantly, these distortions are easily reflected by the sudden change in the lateral offset measurements. Therefore, by identifying the sudden change of the lateral offset measurement, the candidates for face dentations are identified. Figure 2.17 shows an example of the distortion in the extracted longitudinal profile along a w-beam where the arrows represent the offset from the profile to the edge of the travel lane at a one ft. interval. It can be noticed that the minor face dentation shows a rapid change in the longitudinal profile, and the corresponding points in the LiDAR point cloud are then labeled as a potential face dentation for the vertical profile evaluation.

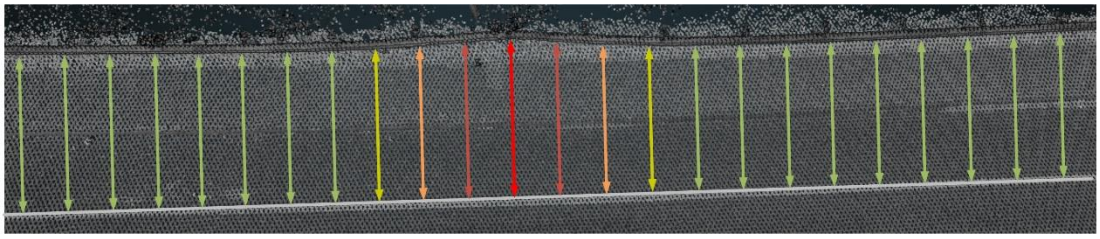

**Figure 2.17: Longitudinal profile at a face dentation**

In this study, the smoothness of the longitudinal profile is introduced to reveal distortions, which are computed based on the first-order derivative. Although investigating the longitudinal profile can efficiently narrow down to the locations where potential face dentations may exist, due to the noise in the lateral offset measurements, not all of the identified locations by this longitudinal profile evaluation step exist actual dentations. For example, as shown in Figure 2.18, two locations were identified: 1) the one

circled in yellow is not a face dentation but a hinge connection that appears to be bending, and 2) the one circled in red is a true face dentation. This longitudinal profile evaluation step will label both locations as candidates. Therefore, a subsequent vertical profile evaluation is needed.

**Figure 2.18: Identified sections with face dentations**

- *Vertical Profile Evaluation*: For the candidate locations where face dentations may exist, a vertical profile evaluation will be conducted to compare the actual vertical profile at this location with a vertical profile that is known to be dentation free. To achieve this goal, the elevation profile (as presented in Subsection 2.4) is reconducted to generate the vertical profile. The vertical profile will be extracted at two locations, including the candidate location identified by the longitudinal profile evaluation and a "neighborhood" location that is known dentation free (i.e., a nearby location where the longitudinal profile evaluation does not label candidates; 10 ft. away from the identified candidate location in this study). It can be observed that the vertical profile at the red location shows a significant shapeshift that is indicative of a face dentation, whereas the vertical profile at the red location does not show any significant shapeshift, which means that no face dentation is present.

  In this study, a Hausdorff (*50*) distance function is defined to measure the shapeshift between the vertical profile at the candidate location and the one that is known dentation free. The Hausdorff distance measures how far two subsets (i.e., both vertical profiles) are from each other. For every point *a* of *A*, find its smallest distance to any point *b* of *B*; finally, keep the smallest distance found among all points *a*.

$$D(A,B) = \min_{a \in A}\left\{\min_{b \in B}\{d(a,b\}\right\}$$

### 2.5.4 Damaged/Missing Terminal Identification

The objective of automatically identifying damaged/missing terminals is to locate the guardrails whose beams have an incomplete or distorted terminal. Therefore, the research team re-introduced the terminal classification method for identifying damaged and missing terminals. As presented in Subsection 2.4, if no OM signs are identified in the video log

image within the projected region of the extracted guardrail-associated point cloud, a BIB terminal or a missing terminal type is assigned to the extracted guardrail. To differentiate the BIB terminal and a damaged/missing terminal, the elevation of the unidentified terminal (i.e., BIB or damaged/missing terminal) was evaluated. For the BIB terminal, since the entire beam is extended into the ground, the elevation of the terminal is often neglectable, while a damaged/missing terminal will render a comparable elevation as the installed beam for the rest of the guardrail. In this study, no damaged/missing terminal was identified in the selected testing sections. However, Figure 2.19 shows examples where different situations other than BIB terminal were identified as damaged/missing terminals, especially the cases where occlusions were observed, e.g., vegetation, mailbox, and data collection artifacts.


**Figure 2.19: Misidentified damaged or missing terminals**

### 2.5.5 Support Deficiency Identification

Figure 2.20 shows a sample dataset for a typical LiDAR scan in this study for the roadside features, including guardrails. It can be observed that, due to the occlusion of the guardrail beams and the scanning angle of the LiDAR sensor, only a limited portion of the guardrail supports can be captured from the point cloud. Therefore, the research team focused on the support deficiency as the missing in this study, and the research team proposed to measure the interval of installed supports and then identify the missing support based on the identified abnormal interval.

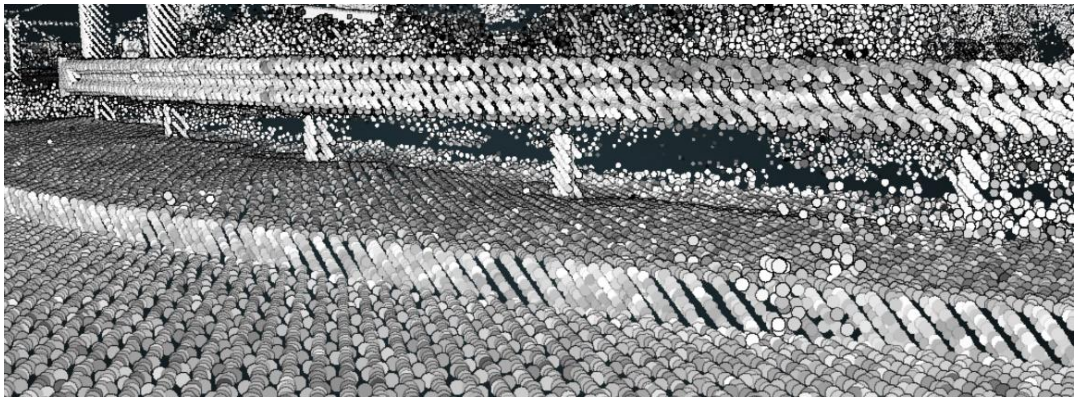

**Figure 2.20: Partially collected guardrail support**

Similar to the vertical profile evaluation approach (as presented in Subsection 2.4), vertical profiles are automatically generated along each extracted guardrail beam. Figure 2.21 shows examples of the vertical profile that is with and without supports. It can be observed that the vertical profile with support shows two distinct clusters that correspond to the guardrail beam and the partial guardrail support, while the vertical profile without support only contains a single cluster that corresponds to the guardrail beam. Therefore, the research team proposes a binary indicator for each extracted guardrail. Each code of the binary indicator represents a sampled vertical profile (at a 1 ft. interval in this study), which is computed by all the points within the 1 ft. interval. If the vertical profile contains a second cluster, then the code "1" is labeled, whereas if the vertical profile does not contain a second cluster, then the code "0" is labeled. Therefore, the installation interval of the guardrail supports can be measured by counting the distance between the two consecutive vertical profiles that are coded "1". With the installation intervals identified for each extracted guardrail beam, a distribution of the interval can be generated. Any interval that is greater than the typical interval (defined as an interval that is larger than 1.5 times the average interval) will be identified as missing support.

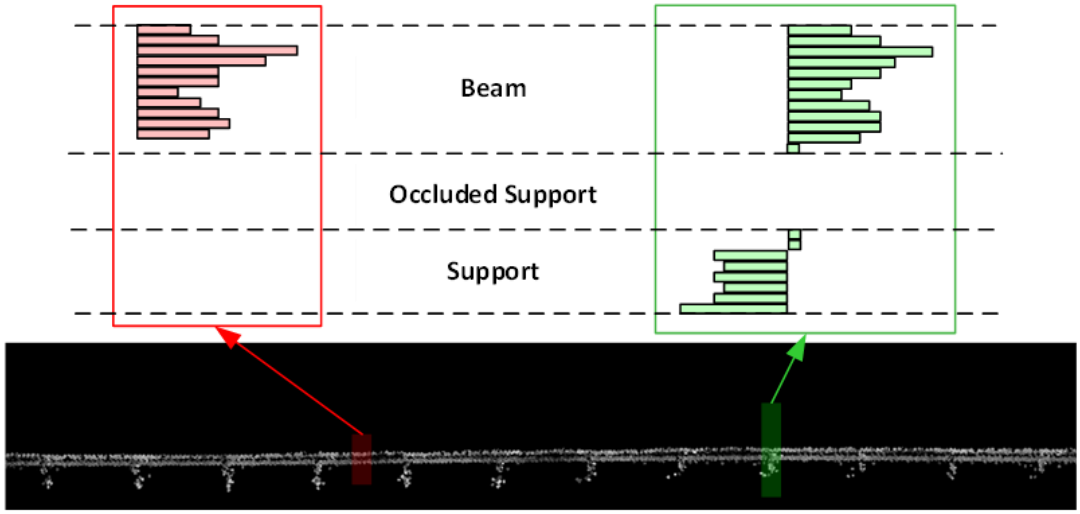


**Figure 2.21: Vertical profiles with and without a support**

### 2.5.6 Exploration of Missing Bolt Identification

The objective of identifying missing bolts is twofold: 1) to identify locations of bolts and bolt holes (if missing), and 2) to determine if a missing or loosened bolt exists. Due to the small dimension of the bolts installed in guardrails, they cannot be typically captured in the LiDAR point cloud data but clearly in the high-resolution video log image. In this study, due to the limited examples of missing/loosened bolts collected from the tested sections, the research team instead explored the feasibility of identifying missing bolts using an existing algorithm and dataset in the structural analysis developed by Yuan et al. (*51*). The algorithm is further

applied to the video log images collected in this study for performance evaluation. Figure 2.22 shows the network adopted from work by Yuan et al. (*51*)using Mask RCNN.

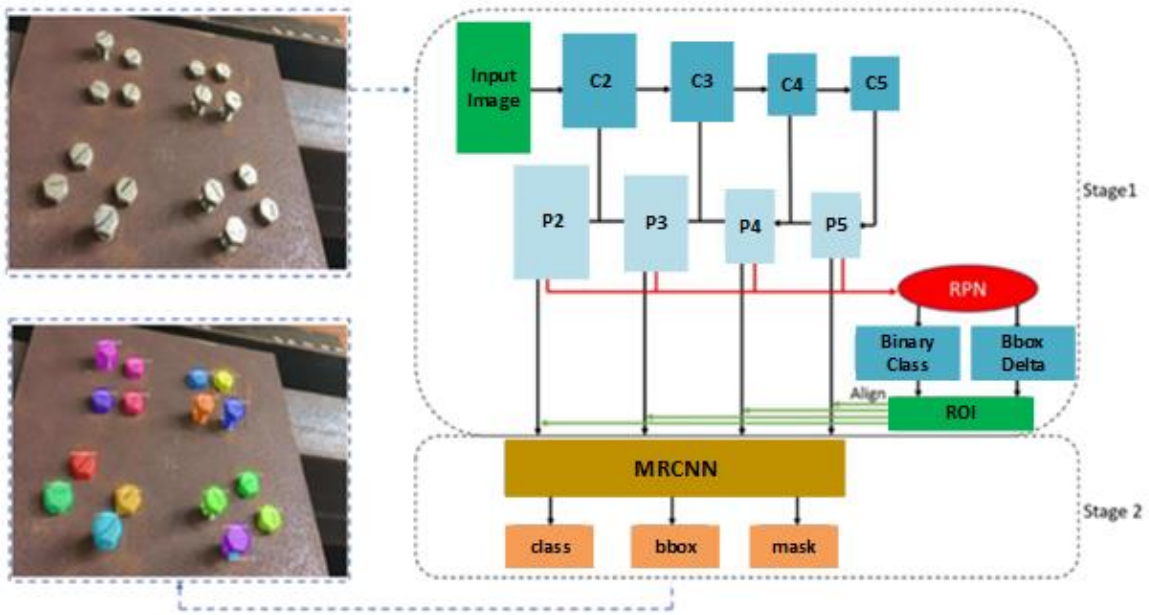


**Figure 2.22: Mask RCNN-based bolt identification algorithm (adapted from (*51*))**

**The framework was proposed in two stages, including the stage for generating object proposals and the second stage for classified proposals to generate bounding boxes and masks. In this study, only the mask branch was implemented for identifying the detailed contours of each bolt. In addition, instead of only segmenting the bolts, the research team proposed to segment the entire scene for the guardrail so that other components of a guardrail can be extracted. Mask RCNN uses the original ResNet architecture for encoding images (*52*). In this study, the original 300 photos used in the study by Yuan et al. (*51*) and an additional 500 video log images from the camera system were prepared for the dataset of training and testing with augmentations (including shift, rescaling, and brightness adjustment). (Blue: Metal beam; Yellow: Wood post; White: Bolt)**

Figure 2.23 shows an example of the segmented results.

**(Blue: Metal beam; Yellow: Wood post; White: Bolt)**

**Figure 2.23: Example of the segmentation results**

While the detection results for in-service bolts showed promises in accurately identifying the locations, it was identified that a higher resolution was required to identify the detailed condition of the bolts (e.g., loosened or missing). Using the video log images from the camera system, depending on the distance between the system and the guardrail, it remains a challenge to capture the detailed conditions. In addition, at a closer data collection distance, the point cloud data was anticipated to capture the geometrical changes for missing or loosened bolts (i.e., missing small bumps on the surface of the guardrail beams). Unfortunately, it is not always ideal for maintaining a close data collection distance to reveal the subtle changes.

This page left blank intentionally.

# 3.0 Results

The results for this study consisted of two main parts: the results from individual algorithm evaluation for guardrail inventory, property extraction, and condition assessment, and an overall performance evaluation for a network-level analysis. Subsections 3.1, 3.2, and 3.3 present the evaluation results that correspond to guardrail extraction, guardrail property identification, and guardrail condition assessment. In this study, given the limited number of testing sections, the parameter sensitivity and the overall inventory results and the guardrail property extraction results were comprehensively evaluated, compared with manual ground truths, whereas the condition assessment results were evaluated with limited samples and visual ground truths.

## 3.1 Guardrail Inventory Algorithm

In this study, the radii pairs, with a scale from 0.0m to 5.0m based on the interval of 0.1m, were used in the DoN calculation of the ground truth points of the guardrail. The guardrail covers a length of 123.14m (0.077 miles) with 44,256 points (Figure 3.1) in a typical area on State Route 113, Dunstable, MA, with a length of 539.18m (0.335 miles) and total points of 9,719,695, as well as including some typical objects, e.g., vehicle, intersection, building, forest zone, etc.

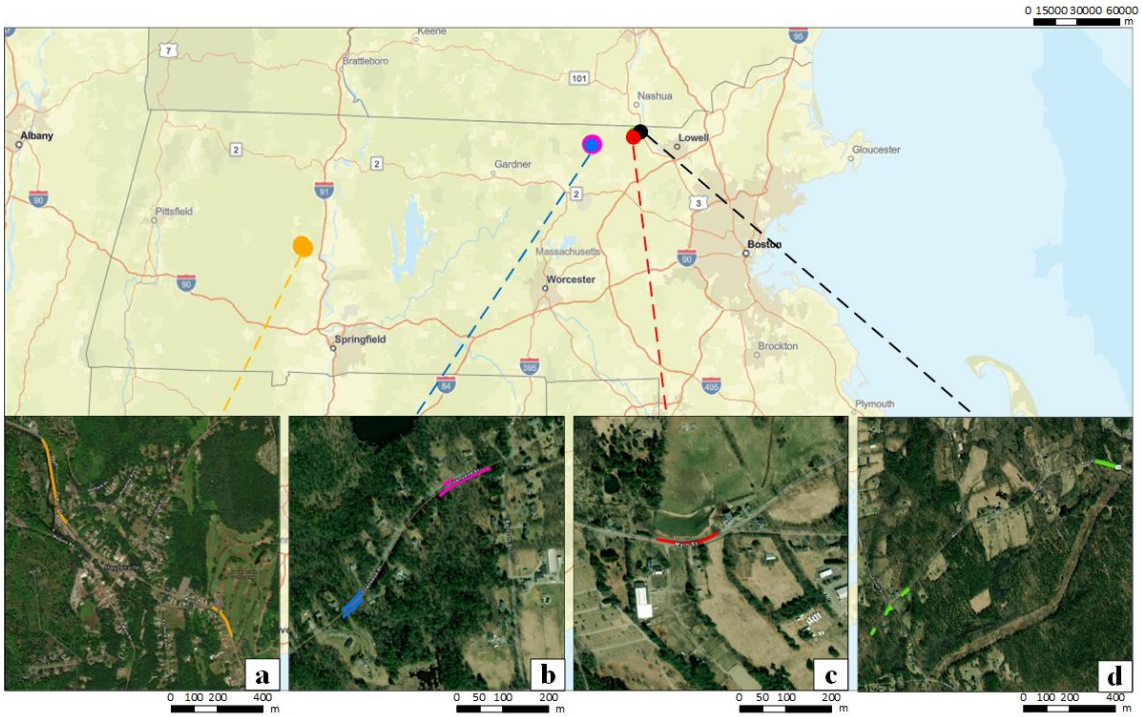


**Figure 3.1: Experimental test areas**

### 3.1.1 Parameters Sensitivity Analysis

In this study, the sensitivity of two sets of critical parameters needs to be evaluated to maximize the overall performance of this proposed method, including the radii values for the DoN-based segmentation step and the voxel sizes in the guardrail-associated point re-population step. This section presents the sensitivity analysis for these parameters.

- *Sensitivity analysis of radii pair.* The proper radii pair $r_1$ and $r_2$ is important for the DoN-based segmentation results. The radii values are used to define the scales of the region where the flatness and surface distortion are investigated so that the local corrugation feature may be revealed. Inspired by the selection algorithm based on the aggregate statistics (median and variance) for the ground truth points of the target object, median and variance are introduced to select the proper radii pair. The median of DoNs is the typical DoN value, which represents how much the local corrugation typically makes the local normal direction depart from the large-scale flat surface. The higher median of DoNs means most of the guardrail points have higher DoN values so that such points could be detected based on their higher DoN values, which are different from the points on the large-scale flat surface. Variance depicts the rate of DoN divergence that reflects how much the local corrugation makes the local normal direction different from the randomly distorted surface. Low variance means there are not many fluctuations in the DoN distribution of the guardrail points, which is different from the points in the randomly distorted surface. Therefore, the primary criteria for radii selection are to identify the radii pair that leads to high median DoN values (orange area as shown in Figure 3.2(a)) and low variance values (blue area as shown in Figure 3.2(b)). The overlapped regions with high median values and low variance values correspond to all the performing radii pairs. However, since the DoN calculation in a large-scale region requires a longer computation time, the radii pair with lower values (i.e., covering a smaller computation region for DoNs) was selected for processing the whole dataset (red circle shown in Figure 3.2(a)).

  In this study, the proper radii pair is 0.2m and 1.2m, with the median value of 0.669 and the variance value of 0.027 according to the criteria. As a result, using the selected radii pair, most guardrail-associated points can be detected with efficient computational cost. It should be noted that the selection of the radii pair for computing DoNs can be sensitive to the density of the point cloud and the corresponding scanning pattern. Therefore, it is recommended that the sensitivity of the radii pair needs to be conducted for other point cloud datasets following the above-mentioned transferable analysis.

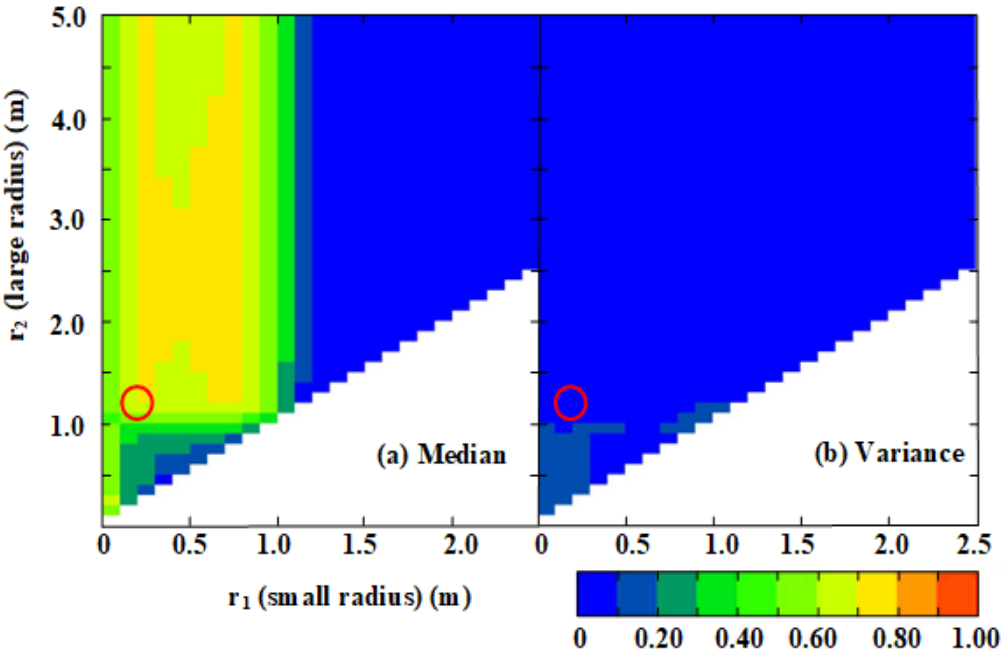


**Figure 3.2: Sensitivity analysis for radii pairs**

- *Sensitivity analysis of voxel size.* To analyze how the voxel size may affect the performance of the guardrail-associated points re-population, different voxel sizes from 0.1m to 2.0m were evaluated. Two areas on State Route 113, Pepperell, MA (as shown in Figure 3.1(b)), were selected as the testing area. The metrics – precision and recall were introduced to analyze the performance of different voxel sizes in the step of the guardrail-associated points re-population. Precision is the proportion of the Predicted Positive cases that are correctly Real Positives, while recall measures the coverage of Real Positive cases by the method which predicts the Positive. Precision and recall are defined as,

$$Precision = \frac{TP}{TP + FP}$$

$$Recall = \frac{TP}{TP + FN}$$

where TP and FP are the True and False Positives (i.e., the number of Predicted Positives that are correct and incorrect, respectively); TN and FN are the True and False Negatives (the number of Predicted Negatives that are correct/incorrect).

The results in the two areas are shown in Figure 3.3(a) and (b), respectively. For Areas 1 and 2, precision and recall are close when voxel size is between 0.2m and 0.3m. More points associated with spacers and posts were re-populated, and fewer interfering points were identified as guardrail-associated points. On the contrary, more points associated with spacers and posts were not detected when the voxel size was smaller, e.g., 0.1m,

which is attributed to the comparable dimensions of spacers and posts captured in this study. Also, more interfering points were detected when the voxel size was larger, e.g., 0.8m, when the voxel started to include points beyond the guardrail beams' proximity. Consequently, the best voxel size should be between 0.2m and 0.3m. Unlike the sensitivity results for the radii pair, because the dimensions for spacers and posts, especially lateral and vertical attachment to the guardrail beams, are universally defined and remain unchanged, the recommended voxel size between 0.2m and 0.3m is transferable for other point cloud datasets.

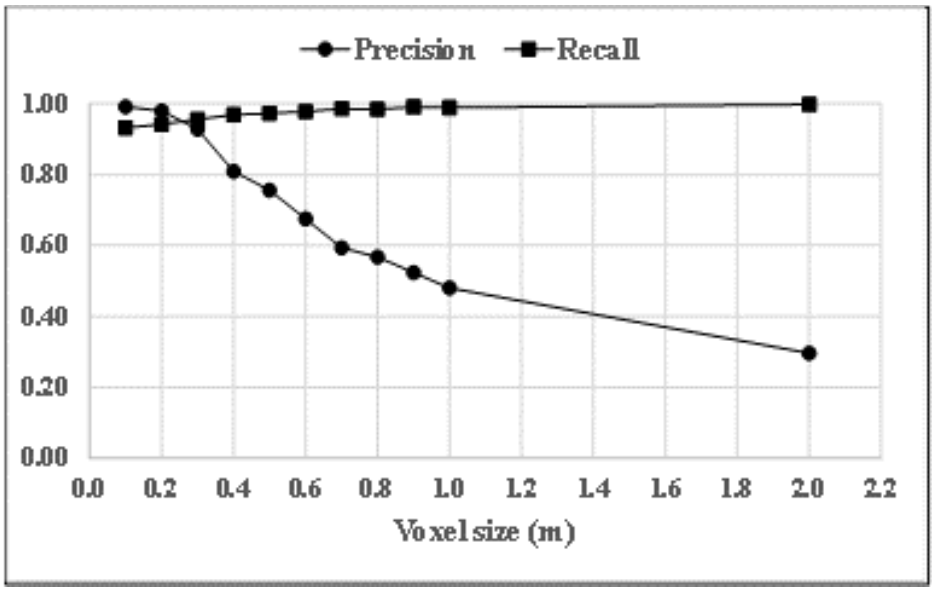


**(a)**

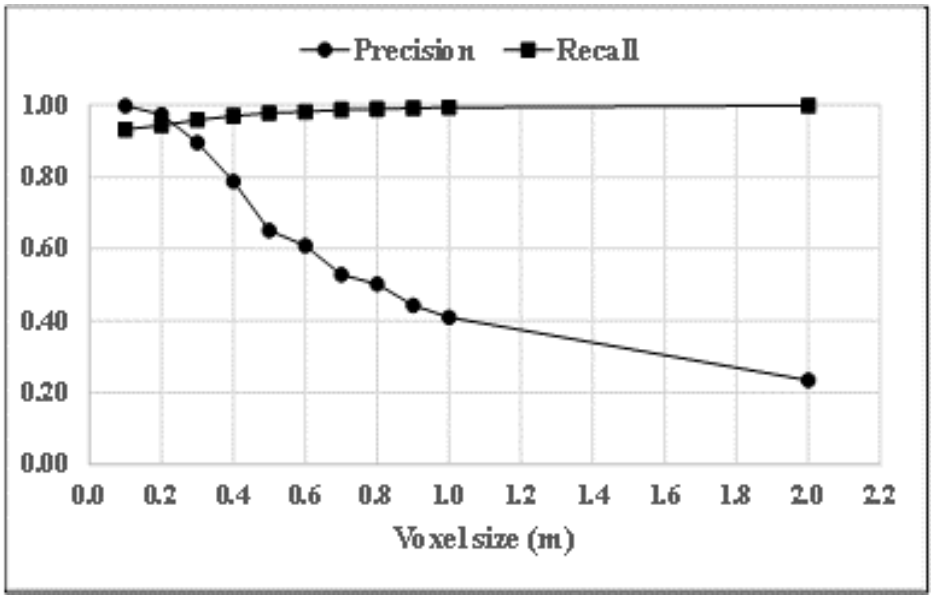


**(b)**

**Figure 3.3: Sensitivity analysis for voxel sizes**

### 3.1.2 Overall Performance

To evaluate the overall performance of the proposed methods, point cloud data collected from two different areas – Area 3 on State Route 113, Dunstable, MA, and Area 4 on State Route 9, Williamsburg, MA, were used in this study.

- The radii pair $r_1$ and $r_2$ are set as 0.2m and 1.2m in DoN-based segmentation. The distance threshold $\Delta_d$ is set as 9.0m based on the double average car length in the guardrail tracking step.
- In Area 3, there is a 2787.06m (1.732 miles) road with a 263.09m (0.163 miles) guardrail, including 78,027 points (green lines as shown in Figure 3.1(d)). Precision is 0.956, and recall is 0.957. The length covering rate is 97.9%. In the Area 4, there is a 1572.05m(0.977 mile) road with 580.23m (0.361 miles) guardrail including 417,227 points (yellow lines as shown in Figure 3.1( (a)). Precision is 0.955, and recall is 0.944. The length covering rate is 100%.

## 3.2 Guardrail Property Identification

To evaluate the overall performance of the proposed method for guardrail property identification, all of the extracted results from Subsection 3.1.1 were used for the subsequent process of extracting the corresponding properties.

- For terminal type identification, three categories of terminals can be successfully extracted and classified, including buried-in-backslope (BIB) terminal, curved terminal (e.g., Modified Eccentric Loader Terminal (MELT), Regent-C, Slotted Rail Termina (SRT-350), etc.), flat terminal (e.g., Flared Energy-Absorbing Terminal (FLEAT), Sequential Kinking Terminal (SKT), Extruder Terminal (ET-Plus), etc.). Out of the tested 427 terminals, the accuracy of the classification rate is 96.4%, with only nine BIB terminals misclassified as curved terminals.
    - In addition, the guardrail beam types of the in-service beam along the tested section on State Route 113 were also extracted and compared with the completed inventory effort by MassDOT. Four types of beam types were compared, including the W-Beam, Thrie-Beam, and double W-Beam and, double Thrie-Beam. The accuracy of the classification is 98.7%, with only less than 1.0% of the double W-Beam sections that were misclassified as Thrie-Beam.
- For geometry property extraction, the developed algorithms can accurately measure the lateral offset and elevations of the guardrail with an average error of less than 1/2 inch. Specifically, by identifying the curb presence, the elevations of guardrails can be measured from the tip to both the pavement surface and the curbed ground with consistent accuracy.

## 3.3 Guardrail Condition Assessment

As presented in previous sections, only a limited amount of testing sections were evaluated in this study, and not all types of conditions were captured from the selected testing sections. Therefore, although the research team developed a suite of algorithms for identifying face dentation, damaged/missed terminal, support deficiency, and missing/loosened bolts, only real-world examples of face dentations were found from the selected testing section. Therefore, this subsection focuses on presenting the details of the face dentation and support deficiency results. While the results for damaged/missed terminal and missing/loosened bolts were not validated by real-world point cloud and video log image data, the results for terminal classification, support identification and interval measurement, and bolt detection are reflective of the performance of the proposed algorithms and their feasibility, respectively.

- The point cloud data collected on State Route 2 were used for evaluating the performance of the developed face dentation algorithm. Along the 5-mile section on State Route 2 near Fitchburg, out of approximately 2.6 miles of guardrails along the shoulder and 4.0 miles of guardrails along the median, there were sixteen small sections containing dentations that were identified using the developed algorithm. A full review of the video log images verified these identified dentations. Figure 3.4 shows some examples of the different magnitude of dentations identified by the developed algorithm.

**Figure 3.4: Examples of the identified face dentations**

- The point cloud data collected on State Route 2 and State Route 9 were used for evaluating the performance of the developed support deficiency algorithm. Only two locations were identified using the developed algorithm. A full review of the video log

images verified these identified deficient supports. It should be noted that the deficient supports were observed to occur with face dentations that indicate a severe impact on the guardrail. Figure 3.5 shows the two locations where deficient supports were identified. It can be observed that the interval of the support changed due to the missing/tilting of the supports.

**Figure 3.5: Examples of identified support failures**

This page left blank intentionally.

# 4.0 Implementation and Technology Transfer

In this study, with feasibility analysis in nature, there was not any immediate implantation or technology transfer plan proposed in the original scope of work. However, the research team worked closely with MassDOT on a case study, which aimed to demonstrate the capacity of the proposed methodology in a network-level analysis. The success of the case study has paved the way for future implementation and technology transfer. The network near Worcester, MA, including Massachusetts State Route 9, State Route 12, and State Route 122 (as shown in Figure 4.1), was selected to demonstrate such a network-level performance.

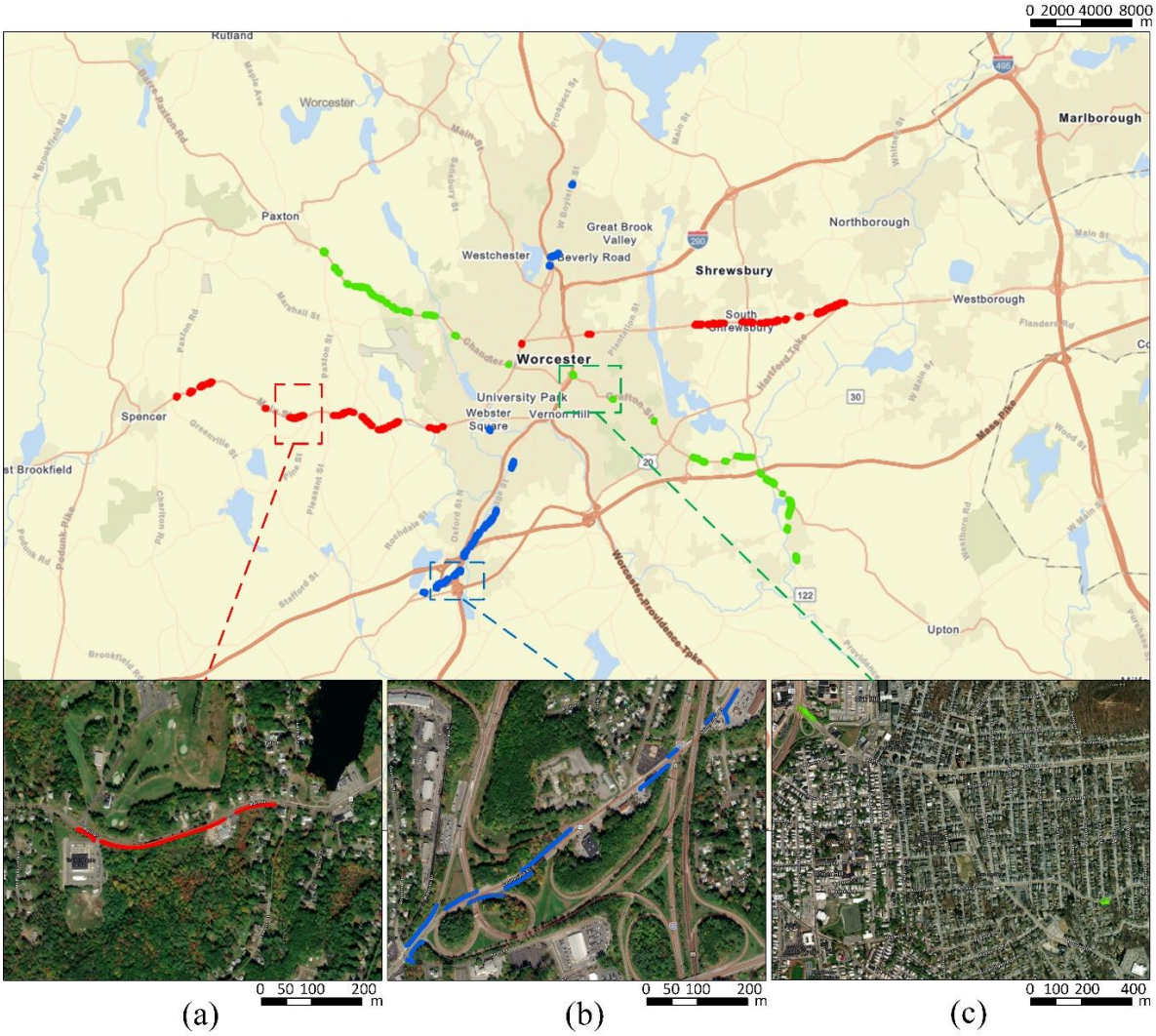


**Figure 4.1: Area of network-level guardrail extraction study**

From the results of the network-level guardrail extraction, there are some conclusions, including 1) the guardrails can be detected and tracked by the proposed model in different

routes with red lines in State Route 9, blue lines in State Route12 and green lines in State Route122; 2) the guardrail can be detected and tracked in different types of the area with rural area (a) in State Route 9, suburban area (b) in State Route 12 and urban area (c) in State Route 122; 3) the proposed model can handle the continuity of the route with long-scale guardrails in the area (a) in State Route 9 and short and discretely distributed guardrails in the area (b) and (c); 4) the guardrails can be detected and tracked by the proposed model in some special area, e.g., tunnels in the area (b) and (c), ramps in the area (b). All the additional results, including the corresponding properties and conditions of the extracted guardrails, were also in a sampled geodatabase.

The productivity (i.e., the processing time) was also evaluated to assess the feasibility of applying the proposed methodology to a statewide process based on this case study. The processing rates for the guardrail inventory, property identification, and condition assessment algorithms are at approximately 150 seconds per mile, 45 seconds per mile, and 60 seconds per mile, respectively. It is anticipated that a full guardrail inventory with detailed property and condition information will only cost a little over 4 min per mile if the developed methodology is successfully implemented.

# 5.0 Conclusions

This study is aimed at developing and validating new processes using automated LiDAR and video-log imagery to identify and extract locations of in-service guardrails and evaluate condition and compliance using representative pilot-testing road sections. Representative testing sections of interstate and non-interstate roadways, with various lengths and guardrail coverages, were selected and analyzed within the study. The detailed objectives include:

- Develop an automated method for determining the presence of guardrails along the roadway and for extracting critical information, including georeferenced starting and ending points, terminal types, curb presence, lateral offset (from the edge of the nearest travel lane to the guardrail), and elevation (from the pavement surface to the tip of the guardrail).
- Develop an automated method for identifying typical conditional changes for guardrails, including face dentation, end terminal damage/missing, and guardrail support deficiency. The research team investigated the feasibility of identifying missing bolts or connection failure of guardrails using image processing.

The deliverables of this study include a georeferenced (and linearly referenced) guardrail inventory for the selected pilot-testing sections, integrating the in-service presence and condition information to support evaluation for MASH compliance and network-level maintenance strategy. **The results show that mobile LiDAR is an effective and efficient technology for network-level guardrail inventory with detailed property and condition information.**

- *A Review of Guardrail Inventory Efforts*. The research team conducted a detailed literature review of available and ongoing research through Transport Research International Documentation (TRID) on guardrail inventory and condition evaluation methods and mobile LiDAR applications, as well as the existing effort of guardrail data collection and inventory that is made by MassDOT.
- *Mobile LiDAR Data Acquisition*. The research team conducted a comprehensive data acquisition and data preprocessing using the mobile LiDAR sensor (i.e., Riegl VMZ-2000) along with the selected, representative, pilot-testing routes.
    - The collected data cover more than 62 miles of different classifications of highways. An additional 15 miles of the network near Worcester, MA, covering State Route 9, State Route 12, and State Route 122, were scanned to demonstrate the overall performance and feasibility of the developed methodology.

- *Guardrail Inventory*. The research team developed fully automated LiDAR processing algorithms for identifying the locations (starting and ending) along the selected pilot-testing routes.
    - The overall performance for the inventory algorithm shows precisions of 0.956 and 0.955 and recalls of 0.957 and 0.944 along the two testing sections on State Route 9 and State Route 113, respectively.
    - The productivity (i.e., the processing time) was also evaluated to assess the feasibility of applying the proposed method to a statewide process. On average, the processing rate for the guardrail inventory algorithm is at approximately 150 seconds per mile.
- *Guardrail Property Extraction*. The research team developed a suite of automated algorithms to extract the detailed properties of the inventoried guardrails, including terminal types, curb presence, lateral offset (from the edge of the nearest travel lane to the guardrail), and elevations (from the pavement surface and ground with curb to the tip of the guardrail).
    - For terminal type identification, three categories of terminals can be successfully extracted and classified, including buried-in-backslope (BIB) terminal, curved terminal (e.g., Modified Eccentric Loader Terminal (MELT), Regent-C, Slotted Rail Termina (SRT-350), etc.), flat terminal (e.g., Flared Energy-Absorbing Terminal (FLEAT), Sequential Kinking Terminal (SKT), Extruder Terminal (ET-Plus), etc.). Out of the tested 427 terminals, the accuracy of the classification rate is 96.4%, with only nine BIB terminals misclassified as curved terminals.
    - For geometry property extraction, the developed algorithms can accurately measure the lateral offset and elevations of the guardrail with an average error of less than 1/2 inch. Specifically, by identifying the curb presence, the elevations of guardrails can be measured from the tip to both the pavement surface and the curbed ground with consistent accuracy.
    - The productivity (i.e., the processing time) was also evaluated to assess the feasibility of applying the proposed method to a statewide process. On average, the processing rate for the guardrail property extraction algorithm is at approximately 45 seconds per mile.
- *Guardrail Condition Assessment*. The research team developed a suite of automated algorithms to assess the conditions of the inventoried guardrails, including face dentation, terminal damage/missing, and support deficiency. The research team also investigated the feasibility of identifying missing bolts or connection failure of guardrails using image processing.
    - For face dentation and terminal damage/missing, the algorithms are evaluated on a 5-mile section along State Route 2, and all of the 16 locations with face dentations and 2 locations with deficient supports were successfully located.

- For terminal damage identification, although no damaged/missing terminals were found in the collected data, the terminal classification algorithm has clearly shown its feasibility of the algorithm. In this study, any terminals that are not identified as BIB, curved or flat terminals will be classified as damaged/missing terminals.
- For missing/loosened bolt identification, although no missing bolts were found in the collected data, the algorithm using datasets collected from previous studies has shown the feasibility of automatically identifying the locations of bolts from video log images using the developed machine learning algorithm. However, due to the configuration of the camera (i.e., the distance between the sensor and the guardrail, the current resolution of 1920x1080 may not be sufficient to identify missing/loosened bolts, and future studies remain needed to further validate the detailed performance of the developed algorithm.
- The productivity (i.e., the processing time) was also evaluated to assess the feasibility of applying the proposed method to a statewide process. On average, the processing rate for the guardrail condition assessment algorithm is at approximately 60 seconds per mile.

The research team has developed a comprehensive methodology for automatically inventorying the locations of the in-service guardrails, extracting the corresponding properties and conditions, and leveraging mobile LiDAR point cloud data and video log images. A case study covering 15 miles of the network (including State Route 9, State Route 12, and State Route 122) near Worcester, MA, was developed to demonstrate the feasibility of the developed methodology for network-level analysis. The resulting inventory geodatabase with all the properties and conditions can be readily used for supporting asset management and safety improvement tasks for MassDOT.

This page left blank intentionally.

# 6.0 References


1. Yin, H., Y. Xiao, G. Wen, and H. Fang. Design Optimization of a New W-Beam Guardrail for Enhanced Highway Safety Performance. *Advances in Engineering Software*, Vol. 112, 2017, pp. 154–164.
2. AASHTO. *Manual for Assessing Safety Hardware*. American Association of State Highway and Transportation Officials, 2016.
3. Wang, Z., Y. J. Tsai, and others. *Exploration of Using GDOT's Existing Videolog Images and Pavement Surface Imaging Data to Support Statewide Maintenance Practices*. Georgia Department of Transportation Office of Research, 2016.
4. Dye Management Group, Inc. *Monitoring Highway Assets with Remote Technology*. Michigan Department of Transportation, 2014.
5. VTrans. *Vermont Agency of Transportation Guardrail Inventory*. 2019.
6. Mason, T., R. Scarr, and K. Perrillo. *Transportation Asset Management System for Roadway Safety: Idaho's Guardrail Management System Saves Lives, Time, and Money (Fact Sheet)*. Federal Highway Administration, 2005.
7. Balali, V., and M. Golparvar-Fard. Segmentation and Recognition of Roadway Assets from Car-Mounted Camera Video Streams Using a Scalable Non-Parametric Image Parsing Method. *Automation in construction*, Vol. 49, 2015, pp. 27–39.
8. Seibert, A., M. Hähnel, A. Tewes, and R. Rojas. Camera Based Detection and Classification of Soft Shoulders, Curbs and Guardrails. 2013.
9. Adam, C., R. Schubert, N. Mattern, and G. Wanielik. Probabilistic Road Estimation and Lane Association Using Radar Detections. 2011.
10. Lundquist, C., U. Orguner, and T. B. Schon. Tracking Stationary Extended Objects for Road Mapping Using Radar Measurements. 2009.
11. Mwakalonge, J. L., J. A. Perkins, and E. C. Jones. Investigating Radio Frequency Identification (RFID) for Linear Asset Management. *Public Works Management & Policy*, Vol. 19, No. 2, 2014, pp. 164–179.
12. Chipengo, U. Full Physics Simulation Study of Guardrail Radar-Returns for 77 GHz Automotive Radar Systems. *IEEE Access*, Vol. 6, 2018, pp. 70053–70060.
13. Zhu, H., F. Chen, and B. Guo. Joint Beam Guardrail Detection and Tracking by Lidar for Real-Time Applications. 2019.
14. Broggi, A., P. Cerri, F. Oleari, and M. Paterlini. Guard Rail Detection Using Radar and Vision Data Fusion for Vehicle Detection Algorithm Improvement and Speed-Up. 2005.
15. Kim, T., and B. Song. Detection and Tracking of Road Barrier Based on Radar and Vision Sensor Fusion. *Journal of Sensors*, Vol. 2016, 2016.
16. Zhu, H., F. Chen, and Z. Wang. A Robust Feature Fusion Method for Camera-Based Highway Guardrail Detection. 2019.
17. Alessandretti, G., A. Broggi, and P. Cerri. Vehicle and Guard Rail Detection Using Radar and Vision Data Fusion. *IEEE transactions on intelligent transportation systems*, Vol. 8, No. 1, 2007, pp. 95–105.
18. Zhao, X., P. Sun, Z. Xu, H. Min, and H. Yu. Fusion of 3D LIDAR and Camera Data for Object Detection in Autonomous Vehicle Applications. *IEEE Sensors Journal*, Vol. 20, No. 9, 2020, pp. 4901–4913.

19. Zhangyu, W., Y. Guizhen, W. Xinkai, L. Haoran, and L. Da. A Camera and LiDAR Data Fusion Method for Railway Object Detection. *IEEE Sensors Journal*, 2021.
20. Tang, H.-L., S.-C. Chien, W.-H. Cheng, Y.-Y. Chen, and K.-L. Hua. Multi-Cue Pedestrian Detection from 3D Point Cloud Data. 2017.
21. Riveiro, B., L. Díaz-Vilariño, B. Conde-Carnero, M. Soilán, and P. Arias. Automatic Segmentation and Shape-Based Classification of Retro-Reflective Traffic Signs from Mobile LiDAR Data. *IEEE Journal of Selected Topics in Applied Earth Observations and Remote Sensing*, Vol. 9, No. 1, 2015, pp. 295–303.
22. Lin, C., Y. Guo, W. Li, H. Liu, and D. Wu. An Automatic Lane Marking Detection Method With Low-Density Roadside LiDAR Data. *IEEE Sensors Journal*, Vol. 21, No. 8, 2021, pp. 10029–10038.
23. Hou, Q., and C. Ai. A Network-Level Sidewalk Inventory Method Using Mobile LiDAR and Deep Learning. *Transportation Research Part C: Emerging Technologies*, Vol. 119, 2020, p. 102772.
24. Zhang, Y., J. Wang, X. Wang, and J. M. Dolan. Road-Segmentation-Based Curb Detection Method for Self-Driving via a 3D-LiDAR Sensor. *IEEE transactions on intelligent transportation systems*, Vol. 19, No. 12, 2018, pp. 3981–3991.
25. Zhu, H., and B. Guo. A Beam Guardrail Detection Algorithm Using Lidar for Intelligent Vehicle. 2018.
26. Jiang, Y., B. He, L. Liu, R. Ai, and X. Lang. Effective and Robust Corrugated Beam Guardrail Detection Based on Mobile Laser Scanning Data. 2016.
27. Gao, J., Y. Chen, J. M. Junior, C. Wang, and J. Li. Rapid Extraction of Urban Road Guardrails From Mobile LiDAR Point Clouds. *IEEE Transactions on Intelligent Transportation Systems*, 2020.
28. Vidal, M., L. Díaz-Vilariño, P. Arias, and J. Balado. Barrier and Guardrail Extraction and Classification from Point Clouds. *The International Archives of Photogrammetry, Remote Sensing and Spatial Information Sciences*, Vol. 43, 2020, pp. 157–162.
29. Hou, S., W. Tan, Y. Zheng, X. Han, and Q. Li. Optimization Design of Corrugated Beam Guardrail Based on RBF-MQ Surrogate Model and Collision Safety Consideration. *Advances in Engineering Software*, Vol. 78, 2014, pp. 28–40.
30. Ioannou, Y., B. Taati, R. Harrap, and M. Greenspan. Difference of Normals as a Multi-Scale Operator in Unorganized Point Clouds. 2012.
31. Rusu, R. B. Semantic 3D Object Maps for Everyday Manipulation in Human Living Environments (Ph. D. Thesis). *Computer Science department, Technische Universitaet Muenchen, Germany*, 2009.
32. Fischler, M. A., and R. C. Bolles. Random Sample Consensus: A Paradigm for Model Fitting with Applications to Image Analysis and Automated Cartography. *Communications of the ACM*, Vol. 24, No. 6, 1981, pp. 381–395.
33. MassDOT. *Updated Standards for Guardrail and Guardrail End Terminals*. Massachusetts Department of Transportation, 2017.
34. Meagher, D. Geometric Modeling Using Octree Encoding. *Computer graphics and image processing*, Vol. 19, No. 2, 1982, pp. 129–147.
35. Zill, D. G., and M. R. Cullen. Definition 7.4: Cross Product of Two Vectors. *Advanced engineering mathematics*, 2006, p. 324.
36. Scarponcini, P. Generalized Model for Linear Referencing in Transportation. *GeoInformatica*, Vol. 6, No. 1, 2002, pp. 35–55.

37. Ray, M., J. Weir, and J. Hopp. *NCHRP 490: In-Service Performance of Traffic Barriers*. National Cooperative Highway Research Program, 2003.
38. AASHTO. *Roadside Design Guide*. American Association of State Highway and Transportation Officials, 2011.
39. Tsai, Y., Z. Wang, and C. Ai. *Implementation of Automatic Sign Inventory and Pavement Condition Evaluation on Georgia's Interstate Highways*. Publication 15–11. Georgia Department of Transportation Office of Research, 2017.
40. Ai, C. *A Sensing Methodology for an Intelligent Traffic Sign Inventory and Condition Assessment Using GPS/GIS, Computer Vision and Mobile LiDAR Technologies*. Georgia Institute of Technology, 2013.
41. Ai, C., and Y. J. Tsai. An Automated Sign Retroreflectivity Condition Evaluation Methodology Using Mobile LIDAR and Computer Vision. *Transportation Research Part C: Emerging Technologies*, Vol. 63, 2016, pp. 96–113. https://doi.org/10.1016/j.trc.2015.12.002.
42. Huang, H., D. Li, H. Zhang, U. Ascher, and D. Cohen-Or. Consolidation of Unorganized Point Clouds for Surface Reconstruction. *ACM Trans. Graph.*, Vol. 28, No. 5, 2009, pp. 1–7. https://doi.org/10.1145/1618452.1618522.
43. Canaz Sevgen, S., and F. Karsli. An Improved RANSAC Algorithm for Extracting Roof Planes from Airborne Lidar Data. *The Photogrammetric Record*, Vol. 35, No. 169, 2020, pp. 40–57.
44. Zhao, G., and J. Yuan. Curb Detection and Tracking Using 3D-LIDAR Scanner. 2012.
45. Hata, A., and D. Wolf. Road Marking Detection Using LIDAR Reflective Intensity Data and Its Application to Vehicle Localization. 2014.
46. Gabauer, D. J., and H. C. Gabler. Differential Rollover Risk in Vehicle-to-Traffic Barrier Collisions. *Annals of advances in automotive medicine. Association for the Advancement of Automotive Medicine. Annual Scientific Conference*, Vol. 53, 2009, pp. 131–140.
47. FHWA. *W-Beam Guardrail Repair and Maintenance*. Publication FHWA-RT-90-001. Federal Highway Administration, 1996.
48. Fitzgerald, W. J. *W-Beam Guardrail Repair: A Guide for Highway and Street Maintenance Personnel*. Publication FHWA-SA-08-002. Federal Highway Administration, 2008.
49. PennDOT. *Shoulder and Guide Rail Condition Survey Field Manual*. Publication PUB 33 (4-22). Pennsylvania Department of Transportation, 2022.
50. Rockafellar, R. T., and R. J. B. Wets. *Variational Analysis*. Springer-Verlog, 2005.
51. Yuan, C., W. Chen, H. Hao, and Q. Kong. Near Real-Time Bolt-Loosening Detection Using Mask and Region-Based Convolutional Neural Network. *Structural Control and Health Monitoring*, Vol. 28, No. 7, 2021, p. e2741. https://doi.org/10.1002/stc.2741.
52. He, K., G. Gkioxari, P. Dollár, and R. Girshick. Mask R-CNN. *arXiv:1703.06870 [cs]*, 2018.